JOURNAL OF PROPULSION AND POWER
Vol. 27, No. 3, May–June 2011

Comprehensive Review of Planar Pulsed Inductive Plasma Thruster Research and Technology

Kurt A. Polzin
NASA Marshall Space Flight Center, Huntsville, Alabama 35812

DOI: 10.2514/1.B34188

Nomenclature

$\mathbf{B}$, B	=	magnetic induction, T
C	=	capacitance, F
$\mathbf{E}$	=	electric field, V/m
E_0	=	initial energy, J
e_0	=	specific energy, J/kg
I	=	current, A
I_{bit}	=	impulse bit, N · s
I_{sp}	=	specific impulse, s
j	=	current density, A/m^2
L	=	dynamic impedance, H/s
L_C	=	coil inductance, H
L_0	=	initial inductance, H
L'	=	inductance per unit length, H/m
L^*	=	inductance ratio
M	=	mutual inductance, H; molecular mass, kg
m_{bit}	=	mass bit, kg/pulse
m_c	=	critical mass, kg
Q_1	=	first ionization potential, J
r	=	radial coordinate, m
R_e	=	external resistance, Ω
R_p	=	plasma resistance, Ω
t	=	time, s
u_e	=	exhaust velocity, m/s
v	=	velocity, m/s
V_p	=	plasma voltage, V
V_0	=	initial charge voltage, V
z	=	axial coordinate, m
z_0	=	electromagnetic stroke length, m
α	=	dynamic impedance parameter
ΔL	=	inductance change, H
η	=	resistivity, Ω · m; efficiency, %
ξ	=	nonpropulsive energy fraction
ρ_A	=	linear mass density, kg/m
ϕ	=	magnetic flux, W
ψ_1, ψ_2	=	critical resistance ratios

Superscript

$*$	=	nondimensional term or critical term

I. Introduction

PULSED inductive plasma thrusters [1] are spacecraft propulsion devices in which energy is capacitively stored and then discharged through an inductive coil. While there are many pulsed inductive plasma accelerator concepts in existence [1–5], this review is limited to a discussion of planar pulsed inductive thrusters (PITs), where the inductive coil takes the shape of a flat spiral (as illustrated schematically in Fig. 1). The thruster is electrodeless, with the time-varying current in the coil interacting with a plasma covering the face of the coil to induce a plasma current. Propellant is accelerated and expelled at a high exhaust velocity ($\mathcal{O}$(10–100 km/s)) by the Lorentz body force arising from the interaction of the magnetic field and the induced plasma current.

Development of an efficient pulsed inductive plasma accelerator is a challenging proposition. Jahn [6] has succinctly stated the following inherent difficulties pertaining to both ionization and acceleration that must be overcome for efficient inductive thruster operation:

> ... inductive discharges embody two inherent electrodynamic disadvantages to conversion efficiency which detract from their propulsive effectiveness. First, any delay in breakdown of the gas after application of the primary field pulse results in energy being dissipated in the external circuit, which, unlike that of the direct electrode devices, is complete without the gas loop... This difficulty might be relieved by providing a separate preionization mechanism or by operation at a sufficiently rapid repetition rate, but it is indicative of an inherent inefficiency in coupling of the external circuit to the plasma.
>
> ...
>
> Equally troublesome is the need to accomplish all the energy input to the gas before much motion of it has occurred. The current induced in the gasloop "secondary" depends on its mutual inductance with the external primary, and thus is a strong function of the physical separation of these two current paths. As they separate under the acceleration, the coupling rapidly becomes weaker.

While the governing physics make the development of a pulsed inductive plasma thruster a difficult prospect, thrusters of this type possess many demonstrated and potential benefits that make them worthy of continued investigation. The electrodeless nature of these thrusters eliminates the lifetime and contamination issues associated

Kurt Polzin has been a propulsion research scientist at NASA's George C. Marshall Space Flight Center since 2004. He received his B.S. in aeronautical and astronautical engineering from Ohio State University in 1999 and his Ph.D. in mechanical and aerospace engineering from Princeton University in 2006, where he was a National Defense Science and Engineering Graduate Fellow. Dr. Polzin has been an author or coauthor of numerous articles on pulsed-plasma propulsion, thruster performance evaluation, and flow components for liquid-metal-fed thrusters and liquid-metal-cooled in-space nuclear reactor systems. He also served as an Adjunct Professor of physics at the University of Alabama in Huntsville in 2007. He is a Senior Member of the AIAA and presently sits on the AIAA Electric Propulsion Technical Committee and the Young Professionals Committee.

Received 24 November 2010; accepted for publication 23 December 2010.

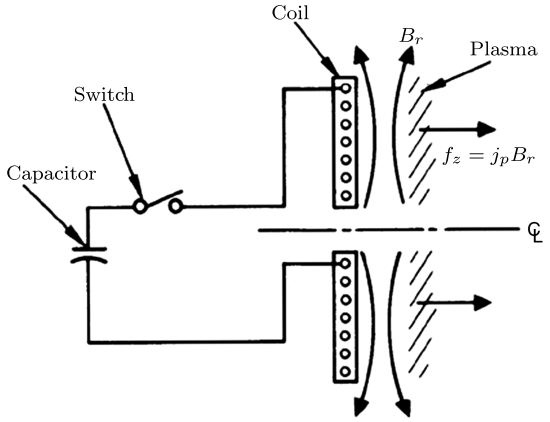

Fig. 1 Schematic showing the basic operation of a planar pulsed inductive plasma accelerator, where j_p is the azimuthal plasma current density (after [1]).

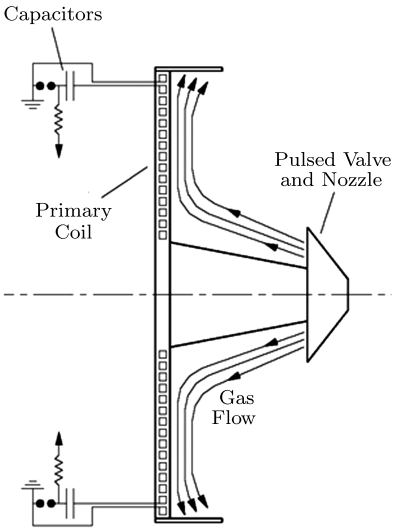

Fig. 2 Schematic showing a typical propellant injection scheme employed on PITs (after [8]).

with electrode erosion in conventional electric thrusters. Also, a wider variety of propellants are available for use when compatibility with metallic electrodes is no longer an issue. Pulsed inductive accelerators have demonstrated operation on propellants like ammonia, hydrazine, and CO_2, and there is no fundamental reason why they would not operate on other propellants like H_2O. It is well known that pulsed accelerators can maintain constant specific impulse I_{sp} and thrust efficiency η over a wide range of input power levels by adjusting the pulse rate to maintain a constant discharge energy per pulse. In addition, PITs have demonstrated operation in a regime where η is relatively constant over a wide range of I_{sp}. Finally, thrusters in this class have operated at high energy per pulse, and by increasing the pulse rate, they offer the potential to process very high levels of power to provide relatively high thrust using a single thruster.

This comprehensive review of planar pulsed inductive plasma accelerator research and development efforts is presented to provide, in one document, a compilation of previous results and a summary of the valuable insights gained through each successive investigation. It is the purpose of this review to provide a common knowledge base that will serve as a reference point for current and future efforts to develop improved PITs. Results are presented to not only highlight beneficial aspects of various design strategies but also to expose deficiencies encountered through past research and development efforts.

In the following section, a review of development work performed up to 1993 on the PIT is presented. The present state of research and development is then discussed, highlighting the various research directions currently being pursued and relating these efforts and their results to past efforts to show how the present research is extracting further physical insight from the historical record.

II. Pulsed Inductive Thruster: 1965–1993

For several decades, research and development of pulsed inductive plasma accelerators were primarily conducted by a small group at TRW Space Systems in Redondo Beach, CA (later acquired by Northrop Grumman Corporation). This work, directed by Dailey and Lovberg [7], included detailed plasma physics studies, component-level development efforts, and performance testing of several different prototypical thruster units, with the goal for each successive step being an inductive thruster operating at higher efficiency than the previous iteration. Historically, the research effort occurred intermittently, with several years elapsing between each undertaking. The PIT Mark (MK) Va developed and tested in the early 1990s represents the culmination of that effort and is presently the most mature and best-performing thruster employing inductive plasma acceleration [7].

The PIT operates in the manner illustrated in Figs. 1 and 2 (after [1] and [8]), where the capacitor bank is charged to high voltage and propellant is injected over the face of the acceleration coil through a nozzle located on the thruster centerline. The capacitors are discharged through the acceleration coil using triggered spark gaps. Current flowing in the coil inductively ionizes the gas, forming a current sheet, and then electromagnetically couples with it to inductively accelerate the current sheet in the axial direction away from the face of the coil, generating thrust.

In the following subsections, we proceed with a chronologically organized developmental history of the PIT, discussing the various design permutations that were tested and showing how they led to the discovery of important physical insights that were employed to increase performance in later iterations, eventually producing the PIT MK Va thruster.

A. Early Research and Development: 1965–1973

During the stages of early research and development, proof-of-concept studies were performed to develop an understanding of inductive current-sheet structure, gain insight into the scaling of thruster performance, and evaluate the efficacy of different techniques for propellant injection and preionization.

1. Inductive Current-Sheet Structure

The earliest research was directed toward understanding the basic microstructure of the current sheet in the planar inductive accelerator geometry [9]. The research focused on determining the plasma acceleration mechanism and quantifying the behavior of ions in the current sheet. This study employed an approach similar to one used by Lovberg when characterizing the microstructure of current sheets in pulsed plasma thrusters (PPTs) and theta-pinch devices [10]. The approach allows not only for the determination of the plasma momentum in both the axial and azimuthal directions but also a temporal and spatial breakdown of the relative contributions of individual acceleration mechanisms to the total momentum.

Measurements of the current sheet were performed on a device possessing a 20-cm-diam coil comprising nine two-turn spirals connected in parallel to a 3.9 μF capacitor bank. The discharge energy was nominally 285 J at a charge voltage of 12 kV. The stray inductance was $\sim$60 nH, while the coil inductance was $\sim$460 nH. Experiments were performed using an ambient argon fill at a pressure of 500 mtorr.

The results of the study are summarized as follows. The axial electric field alone was sufficient to accelerate the ions to the observed sheet speed. This field was due to a combination of the charge separation (polarization field) between the ions and the accelerating electrons that were carrying the current j_θ, and the large negative electron pressure gradient at the leading edge of the sheet, which served to enhance the axial electric field. There was very little

additional acceleration on the trailing side of the current sheet, where the $j_\theta B_r$ force is mostly balanced by the positive electron pressure gradient and serves only to maintain the sheet's cohesiveness. The ions do not acquire momentum in the azimuthal direction and, consequently, do not carry current, because the force exerted on the ions by the induced, azimuthal electric field E_θ was balanced by the resistive drag of the current carrying electrons.

These data superseded the results of earlier studies [11–13], which concluded that ions did carry a substantial portion of the current. The authors noted that the assumptions made in the analysis of the Stark broadening data in those earlier studies [14], specifically assuming constant **E** and **B** fields, were violated in the inductive accelerator current sheet and resulted in misleading conclusions [9].

2. *20-Centimeter Accelerator Performance*

Concurrent with their current-sheet physics investigations, the TRW group performed exploratory research to study the effect of various operational permutations on performance [15]. The first accelerator evaluated was the same 20-cm-diam accelerator described in the previous section and shown in Fig. 3. It was designed to have a bank capacitance of either 3.9 or 1.75 μF, with a nominal charge voltage of 12 kV. The inductance rose over a plasma travel distance (electromagnetic stroke length) of 2 cm from an initial value of ~100 to ~500 nH, which are slightly different inductance values than those given in [9]. Experiments were performed using both a static-fill and pulsed gas injection. In the cases where pulsed gas injection was employed, the valve was open for approximately 200 μs, releasing a mass bit of roughly 200 μg/shot. Both argon (Ar) and nitrogen (N_2) propellants were tested in this accelerator. Experiments were also performed with a 0.04 μF capacitor connected across the acceleration coil terminals. When the main bank was discharged through a spark-gap switch, the smaller capacitor quickly charged, overshooting the initial voltage on the main bank and resulting in a voltage across the coil terminals that was ~1.3 times the initial voltage on the main bank.

An electric thruster's performance is typically defined by the accelerator efficiency η and the specific impulse I_{sp}. For a pulsed electric thruster, these are defined as

$$\eta = \frac{m_{bit}u_e^2}{2E_0} = \frac{I_{bit}^2}{2m_{bit}E_0}, \qquad I_{sp} = \frac{u_e}{g_0} = \frac{I_{bit}}{m_{bit}g_0} \tag{1}$$

The performance of the 20 cm accelerator, measured using a thrust balance, is plotted in Fig. 4a for a static backfill and a capacitance of 1.75 μF. Performance at a bank capacitance of 3.9 μF is plotted in Fig. 4b for a static backfill with inductive overshoot and for pulsed gas injection without inductive overshoot. A maximum efficiency of 11% was achieved at an I_{sp} of 1500 s, with greater efficiencies achieved when inductive overshoot was employed. Additionally, the

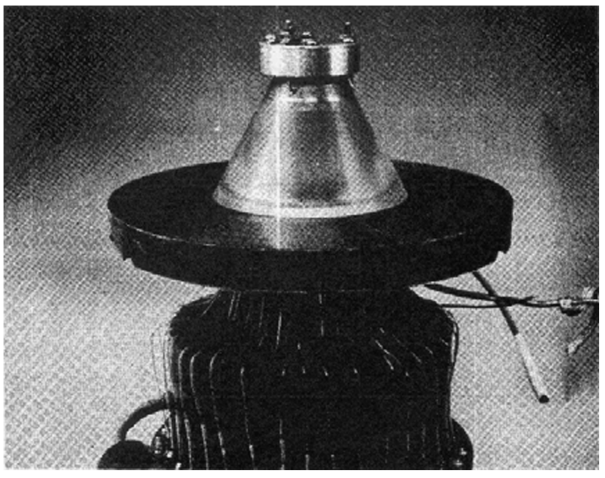

Fig. 3 Photograph of 20 cm pulsed inductive accelerator (from [15]).

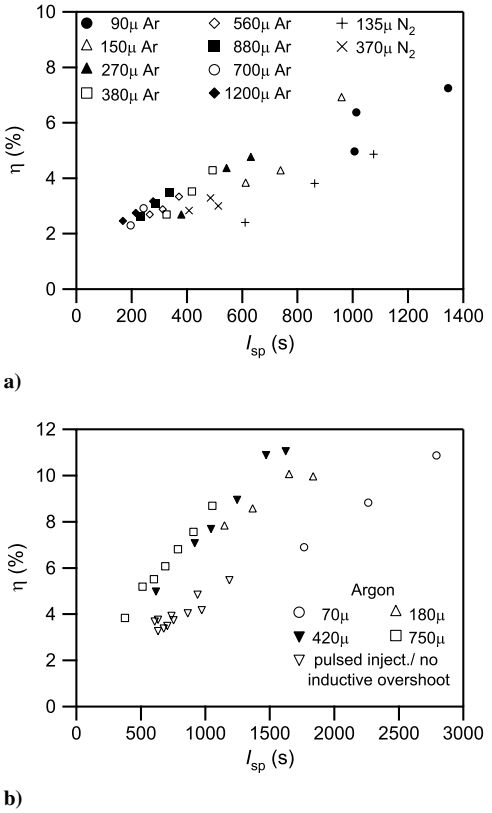

Fig. 4 20-cm-diam thruster performance: a) static-fill, 1.75 μF; and b) inductive overshoot or pulsed gas injection, 3.9 μF (from [15]).

slope of the pulsed gas injection performance data is comparable to the static-fill cases where no inductive overshoot was employed. The differences in the bank capacitances for the two graphs presented in Fig. 4 did not permit a more general comparison of performance scaling between the data sets.

3. *30-Centimeter Accelerator Performance*

Following tests with the 20-cm-diam accelerator, a 30-cm-diam version [16] was fabricated and tested. This thruster had a capacitance of 6 μF, with a discharge energy of 675 J/pulse at a nominal charge voltage of 15 kV. The acceleration coil consisted of 12 two-turn spirals, each connected in parallel to the capacitor bank, producing a coil inductance of roughly 680 nH. Performance was estimated using probes to measure the current density and magnetic field in the r-z plane, with thrust calculated from the measurements by computing the $\mathbf{j} \times \mathbf{B}$ body force and integrating throughout the volume [assuming a two-dimensional (2-D) axisymmetric profile].

Testing was performed using three different propellants (N_2, Ar, and Xe). Gas was introduced as either a static fill or through pulsed gas injection with a nominal injected mass bit of 1.8 mg/shot. The pulsed gas propellant distribution on the face of the inductive coil at this mass bit was measured using an ionization gauge and found to be nonuniform, which may have led to reduced performance. Propellant preionization methods employed a second capacitor charged to 15 kV and discharged just before the main capacitor bank using an independently triggered spark-gap switch. The four preionization variations (methods) were 1) a 0.44 μF capacitor discharged through the acceleration coil; 2) a 0.04 μF capacitor discharged through the acceleration coil; 3) a 0.44 μF capacitor discharged through a 30-cm-diam circular loop of wire located axially 5 cm downstream from the acceleration coil; and 4) a 0.44 μF capacitor discharged through an open, mirror image of the main coil located axially 4 cm downstream from the acceleration coil.

The best performance measurements obtained on the 30 cm accelerator for each of the various operational permutations are summarized in Table 1. The data indicate that the cases of static fill

Table 1 Best thruster performance computed from field measurements for a 30-cm-diam accelerator operating under different combinations of propellant type and injection and using different preionization schemes (from [16])

Gas	Static fill	Pulsed injection	Preionization method	η, %	I_{sp}, s
Ar	Y (500 mtorr)	N	None	17	1430
Xe	N	Y	None	4	500
Xe	N	Y	1	<4.5	——
Xe	N	Y	2	4.5	——
Ar	N	Y	3	7	800
Ar	N	Y	4	18	1470

with no preionization and pulsed gas injection using preionization method 4 have the highest performance. Both were greater than that obtained on the 20 cm accelerator, although we note that the 30 cm accelerator also had a higher charge voltage, discharge energy, and coil inductance. Passing the preionization pulse through the acceleration coil (preionization methods 1 and 2) with pulsed gas injection did not show any improvement over the nonpreionized case, with all three cases significantly underperforming the 20 cm accelerator.

Data presented in Fig. 5a compare the current density in pulsed gas injection cases with a static-fill case. Preionization was not employed for these trials. We observe that the current density in the pulsed gas injection cases is both lower and very nonuniform, leading to a smaller overall acceleration force on the propellant. In separate testing, the pulsed gas mass bit was raised and the uniformity of the initial gas distribution and current density did improve, although it still remained below the static-fill values.

Data plotted in Fig. 5b show the volume-integrated force as a function of time for various cases. The total impulse (time integral of the force) and commensurate performance were greatest for the static argon fill and the pulsed argon mass injection with preionization method 4. The transient (pulsed injection) Xe cases possess a much lower thrust, with the force rising much more slowly in the nonuniform gas distribution case than in the higher mass bit, more uniform case, although the force eventually peaked at roughly the same value in both cases. Finally, the data show that the force peaks more sharply, rising to a higher level when the propellant is preionized by some method.

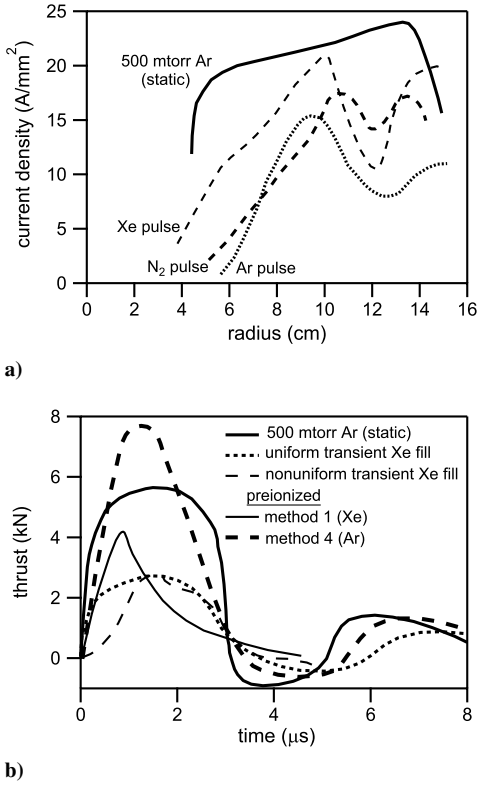

Fig. 5 30-cm-diam thruster measurements: a) maximum current density, $z = 1$ cm downstream, no preionization; and b) thrust histories from field measurements (from [16]).

These results show that a precursor current pulse passing through the main coil (methods 1 and 2) did preionize the gas, but the fields created by this preionization pulse immediately began to accelerate the propellant away from the coil. Consequently, the plasma had already moved some distance away from the coil face before the main acceleration pulse was initiated, reducing the overall potential for inductive acceleration. When preionization method 4 was employed, a preionized current sheet was launched toward the acceleration coil, compressing the propellant against the acceleration coil face and allowing for greater coupling between the acceleration coil current and the plasma sheet. Although this yielded the best I_{sp} and η of any case tested, a preionization coil in the plume of the thruster would not be retained as a design option in future development, because it would experience severe erosion due to ion bombardment over the duration of a mission.

4. Summary of Important Results

Research during this initial period of development produced the following key results:

1) Charge separation in the current sheet produces an axial electric field that serves to accelerate the ions.

2) The induced current in the current sheet is only carried by electrons, since the ions do not acquire azimuthal momentum.

3) Performance in the 20 cm accelerator was improved in the configuration that employed inductive overshoot in the current pulse.

4) The 30 cm accelerator outperformed the 20 cm accelerator in the static-fill case.

5) The 30 cm accelerator employing pulsed gas injection had lower performance and produced a current sheet that was significantly weaker and more nonuniform relative to the static-fill case.

6) In the 30 cm accelerator, the use of preionization schemes passing a current pulse through the coil in advance of the main discharge did not improve the performance relative to the cases where no preionization was employed.

B. Propulsion System Development: 1979–1984

The focus of PIT work during this time period was the development of a full-scale engineering model of the PIT and the derivation of a relatively simple inductive thruster plasma acceleration model.

1. Hardware Development

During this time period, development centered around a revised base thruster design. The biggest change implemented in this new design was an increase of the acceleration coil diameter to 1 m, which studies indicated would substantially increase the electromagnetic coupling distance, improving performance [17]. The thruster possessed a coil comprising 36 one-turn spiral wires connected in parallel to a 20 μF capacitor bank. The bank stored 4 kJ of energy per pulse (at 20 kV nominal charge) and was switched using a triggered spark gap. Pulsed mass injection systems were used exclusively by

Table 2 Performance data for a 1-m-diam 20 μF PIT operating on argon propellant [1,18,19][a]

m_{bit}, mg	Energy, J	I_{sp}, s	η, %	Measurement
		From [1]		
15	4000	1540	42	Probe
7.5	4000	2240	50	Probe
		From [18]		
14.5	3240	1100	24	Probe
13.5	4000	1370	30	Probe
13.8	4840	1580	33	Probe
13.6	5760	1870	40	Probe
		From [19]		
17	4840	1620	44	Probe
17	4840	1236	25.4	Thrust stand

[a]Performance was measured in each case using the indicated method.

the TRW group from this point forward, since an ambient fill is not possible in a real thruster. Propellant preionization was not used during any of the experiments of this time period.

Performance measurements for this thruster are summarized in Table 2 and plotted in Fig. 6. Thruster performance was primarily calculated by a probe method where the distributions of current density and magnetic field were measured, and then the Lorentz body force was computed and integrated over both the discharge volume and the pulse length [1,18,19]. As noted in Table 2 (and discussed further next), in one case, a thrust balance method was used to provide a direct performance measurement. For this case, an additional measurement was performed using a magnetic pressure method where the difference in $B_r^2/2\mu_0$ integrated over the front and back coil surfaces provided a value for the impulse per pulse [19]. This method, which was not further pursued or validated, agreed with the thrust balance method to within 1%.

All the data from this time period indicated that the 1-m-diam coil had improved performance relative to the 20 and 30 cm designs of the 1970s. The data from [1] indicated exceptional performance, with an accelerator efficiency of 50%, but later additional data [18] fell well below these original performance measurements. Lovberg and Dailey [18] believed the later data were more reasonable, owing to a nonuniform initial gas distribution over the coil face. Specifically, they found a region of lower density at smaller radii that could leave the coil in that region unloaded, leading to an increase in the effective initial inductance. An insightful comparison can be made between the probe evaluation method and thrust balance measurements found in [19]. We observe in Table 2 and Fig. 6 that the performance measured on the thrust stand falls well below that calculated from field measurements. This suggests that the integral of the Lorentz body force should not be used to evaluate PIT performance, as it appears to overstate both I_{sp} and η. After these measurements, the performance of PITs was exclusively evaluated using a thrust balance.

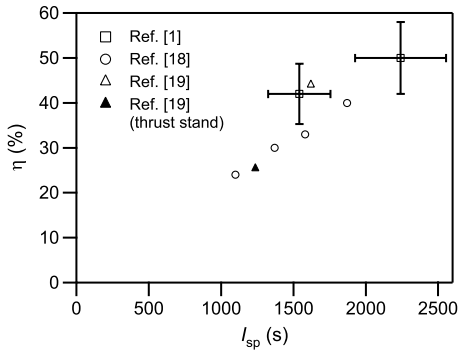

Fig. 6 Performance data for a 1-m-diam 20 μF PIT operating on argon propellant (from [1,18,19]), corresponding to the data found in Table 2.

2. Thruster Performance Model

A circuit-based model of a pulsed inductive accelerator was introduced during this time period to aid thruster design [1,17]. The model consists of a set of circuit equations that are coupled to a one-dimensional (1-D) momentum equation, with thruster performance predicted through numerical solution of the equation set. In general, the thruster performance predicted by the model agreed with thrust stand measurements, and the model was able to provide physical insights into thruster operation. We proceed with a brief review of the model, referring the reader to the literature for a more detailed discussion [1,7,17].

A lumped-element circuit model of a pulsed inductive accelerator is presented in Fig. 7a. The two circuits are inductively coupled through the acceleration coil, which acts as a transformer with mutual inductance $M(z)$, where z is the current sheet's axial position. The circuit can be redrawn as the equivalent circuit, shown in Fig. 7b, with a time-varying behavior governed by the following coupled set of first-order ordinary differential equations:

$$\frac{dI_1}{dt} = \frac{VL_C + (MI_1 + I_2L_C)(dM/dt) - I_2MR_p - I_1R_eL_C}{L_C(L_0 + L_C) - M^2}$$
$$\frac{dI_2}{dt} = \frac{M(dI_1/dt) + I_1(dM/dt) - I_2R_p}{L_C} \qquad \frac{dV}{dt} = -\frac{I_1}{C} \tag{2}$$

where V is the voltage on the capacitor. Based on experimental measurements [1], it was found that the time variation in the mutual inductance can be modeled using the differential equation

$$\frac{dM}{dt} = -\frac{L_C}{2z_0}\exp\left(-\frac{z}{2z_0}\right)\frac{dz}{dt} \tag{3}$$

where z_0 is defined as the electromagnetic decoupling length.

An idealized "snowplow" mass accumulation model is employed, with the thin current sheet generated near the inductive coil entraining and accelerating the gas that it encounters as it moves downstream. The propellant mass in the current sheet as a function of time can be written as

$$m(t) = m_0 + \int_{t=0}^{t} \rho_A v_z \, dt \tag{4}$$

where ρ_A is the linear (axial) mass density distribution, and v_z is the sheet velocity. The term m_0 represents the initial mass of propellant in the sheet, while the integral term represents the mass accumulated by the sheet as it moves away from the acceleration coil. The corresponding momentum equation for this system can be written as

$$\frac{L_C I_1^2}{2z_0}\exp(-z/z_0) = \rho_A v_z^2 + m(t)\frac{dv_z}{dt} \tag{5}$$

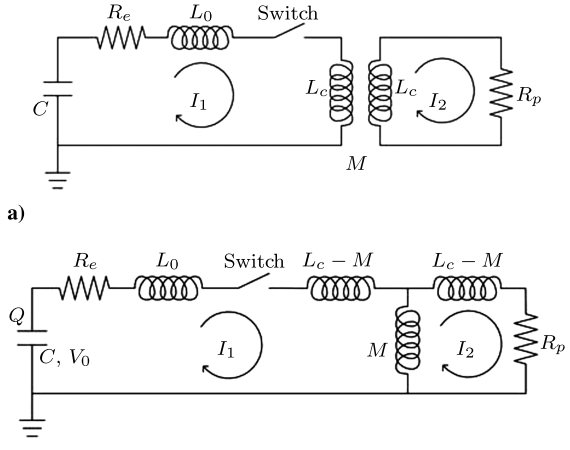

Fig. 7 Circuit models: a) general lumped-element representation of a pulsed inductive accelerator and b) equivalent circuit (after [1]).

The left-hand side represents the self-field electromagnetic force, while the first term on the right-hand side is the momentum investment associated with entraining the propellant and the second term represents further acceleration of the already entrained propellant.

In this simplified, 1-D model, the need for an energy equation was eliminated by explicitly assuming a value for the electron temperature to yield a match between the experimental performance data and numerical simulations. This assumption allowed for the approximate computation of the plasma resistance R_p.

The model provided two important insights into PIT operation [8]. First, it predicted an operational regime where the efficiency would be relatively constant over a broad range of I_{sp} values. Second, it showed that matching of the electrical circuit and propellant acceleration timescales was necessary to obtain optimum efficiency.

3. *Summary of Important Results*

The following key results were obtained during this period of development:

1) Performance of the 1-m-diam thruster was significantly improved relative to the 20- and 30-cm-diam accelerators.

2) The field-mapping method produced performance measurements that were much higher than those obtained using a thrust stand, leading to a general rejection of the field-mapping technique in all future work.

3) A circuit-based performance model was introduced and generally agreed well with thrust stand measurements.

4) The model predicted parameter ranges where the thruster efficiency is relatively constant. It also showed that this would occur when the electrical circuit and propellant acceleration timescales were approximately matched.

C. Propulsion System Development: 1987–1989

In the late 1980s, two new thruster models, the PIT MK I [20] and MK IV [21], were fabricated and tested. In addition to studying the effect of changing bank capacitance on thruster performance, the standard resistive inductive capacitive (RLC) circuit was modified in the MK IV to permit the use of a diode clamps, which were used to minimize voltage reversal on the capacitor bank. We proceed with descriptions of the MK I and MK IV designs, followed by a presentation and discussion of performance measurements.

1. *Thruster Descriptions*

The PIT MK I thruster was roughly the electrical equivalent of the thruster described in Sec. II.B. It possessed a 1-m-diam coil comprising 36 one-turn spirals connected in parallel to a 20 μF capacitor bank. The accelerator was also operated using a 10 μF capacitor bank. The parasitic circuit inductance was ~60–80 nH, while the coil had an inductance of 700 nH and an electromagnetic stroke length of 12 cm. Over the outer 6 cm radius, the pitch of the coils was decreased to double the current density in that region, compensating for the loss in magnetic pressure due to field fringing. Current was switched using a triggered spark gap. The thruster was operated in a ringing mode, consistent with the underdamped solution to an RLC circuit. The dual-cone nozzle used in this design was a new feature, and it served to increase the uniformity of the propellant distribution over the face of the acceleration coil. A plot of the constant pressure contours for this propellant injection configuration obtained 1.25 ms after the gas injection valve was opened is presented in Fig. 8.

The MK IV thruster differed from the MK I in several ways. The diameter of this thruster was only 67 cm, and the coil comprised 24 single-turn spirals. The power bus was designed to allow for easy insertion of a diode clamp into the circuit, as shown schematically in Fig. 9. The diode clamp was employed to keep the voltage on the capacitor bank from reversing, thus maintaining and prolonging the initial current pulse and reducing the likelihood of a secondary discharge if the voltage did reverse. The thruster was operated in both the diode-clamped and ringing modes, and it was tested at bank capacitances of 5.8, 13.4, 17.4, and 28.7 μF.

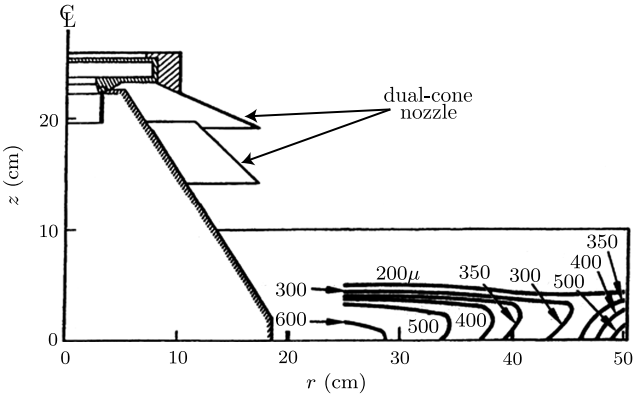

Fig. 8 Experimentally determined constant gas pressure contours in the PIT MK I for a dual-cone nozzle 1.25 ms after opening the gas injection valve (from [20]).

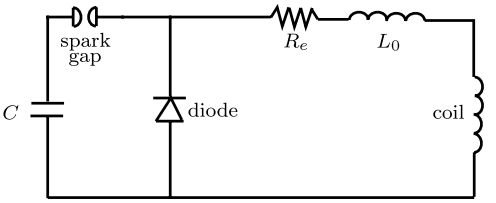

Fig. 9 Circuit schematic for the PIT MK IV operating in the diode-clamped configuration.

2. *Thruster Performance*

Performance data from the PIT MK I and MK IV are presented in Fig. 10 (after [20–22]), and additional MK I data obtained at a bank capacitance of 20 μF are given in Table 3. These data are based on impulse measurements obtained using a thrust balance. These data show that, at the same charge voltage, the performance improved with increased capacitance. In general, the performance also increased with increasing discharge energy and decreasing mass bit. For the same charge voltage, the I_{sp} of the MK I thruster with ammonia (NH_3) propellant was generally higher than with argon. From Fig. 10, we observe that the MK IV thruster provided lower performance with Ar than the MK I. In addition, the diode-clamped version of the MK IV had even lower performance than that without a diode clamp.

Insight into the markedly lower MK IV performance can be gained from induced magnetic field measurements, which were obtained at several axial locations for both the MK I (Fig. 11a) and MK IV (Fig. 11b) thrusters operated in ringing mode. In the MK IV, all the induced field waveforms initially increase at $t = 0$, indicating rapid

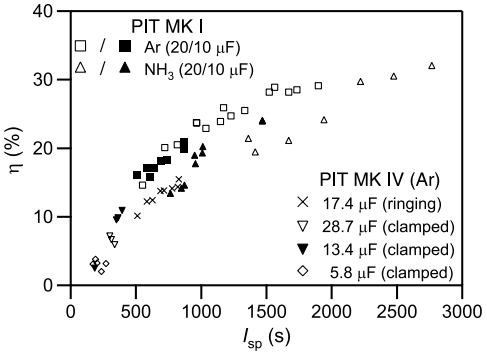

Fig. 10 Performance data from the PIT MK I and MK IV thrusters (after [20–22]).

Table 3 Performance data from the PIT MK I operating at a bank capacitance of 20 μF (from [20])

m_{bit}, mg	Energy, J	I_{sp}, s	η, %
	Ar propellant		
12	5760	1734	28.5
12	6760	1897	29.1
15	5760	1562	28.9
15	6760	1670	28.2
18	3240	964	23.7
18	5760	1334	25.5
18	6760	1521	28.2
20	5760	1228	24.7
23	5760	1171	25.9
26	2560	551	14.6
26	3240	721	20.1
26	4000	816	20.5
26	4840	966	23.7
26	5760	1036	22.9
26	6760	1147	23.9
	NH_3 *propellant*		
5	4000	2220	29.6
5	4840	2476	30.4
5	5760	2766	31.9
6.5	4000	1670	21.0
6.5	4840	1940	24.0
12	4840	1360	21.3
12	5760	1413	19.3

resistive diffusion of the magnetic field through the plasma (low conductivity). In the MK I, the sharp increases generally occur at different times, which is indicative of a high conductivity current sheet passing the spatial locations. The MK I waveforms also increase more rapidly and to greater peak values due to the lower initial inductance and higher energy per pulse relative to the MK IV. The MK IV shows additional current sheets forming after the first half-cycle, indicated by the divergence of the traces at ~6.5 and 20 μs. This "crowbarring", which was not observed in the MK I, implies that the first current sheet did not effectively sweep the plasma out of the acceleration region, thus allowing for coupling between the external circuit and the remaining gas during circuit ringdown. It was concluded that the higher parasitic inductance found in the MK IV reduced the initial current rise rate, dI/dt, leading to an incomplete or nonuniform breakdown during the first half-cycle relative to the MK I.

The lower performance of the diode-clamped MK IV relative to the ringing MK IV was not discussed in the literature. However, these can be understood using the ringing-mode MK IV magnetic field traces in the second half-cycle of the discharge (Fig. 11b, beginning near 6.5 μs). In this part of the discharge, the magnetic field traces associated with a well-formed current sheet can be seen. As this sheet sweeps the propellant, it provides additional propulsive benefit to the thruster (although not as great a benefit as in the MK I where the propellant was swept during the first half-cycle). In the diode-clamp configuration, the severity of the current reversal is mitigated, reducing the current rise rate and peak level flowing in the acceleration coil during the second half-cycle. Consequently, after current reversal, we expect the diode-clamped configuration to produce a weaker current sheet, yielding less propulsive benefit relative to the ringing MK IV, which is the observed result in Fig. 10.

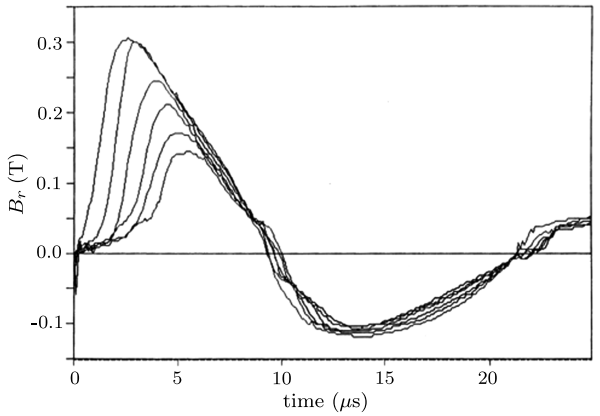

a)

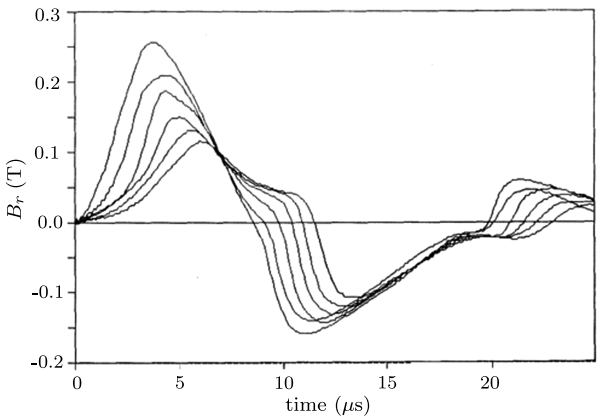

b)

Fig. 11 Magnetic field measurements, $z = 1$, 2, 3, 4, 5, and 6 cm: a) MK I, 20 μF; and b) MK IV, 17.4 μF, ringing mode (from [21,22]).

3. Summary of Important Results

Development efforts during this period of development produced the following key results:

1) The MK I thruster generally outperformed the MK IV variant and, at a fixed charge voltage, the MK I operated at higher I_{sp} when the propellant was ammonia instead of argon.

2) Performance in the MK IV thruster was reduced by incomplete current-sheet formation, which resulted from a lower current rise rate owing to an increase in stray inductance and a lower initial energy per pulse relative to the MK I.

3) Diode clamping in the MK IV thruster reduced current reversal in the pulse circuit, leading to weaker secondary current sheets, which were imparting significant additional momentum to the propellant in the ringing MK IV.

D. Propulsion System Development: 1991–1993

The lessons learned in the 1980s gave rise in the early 1990s to the PIT MK V design [7,8,23], which is shown in Fig. 12. Testing with the MK I and MK IV thrusters highlighted the importance of having a high initial current rise rate, dI/dt, in the coil to form an impermeable current sheet during the first half-cycle of the discharge that could

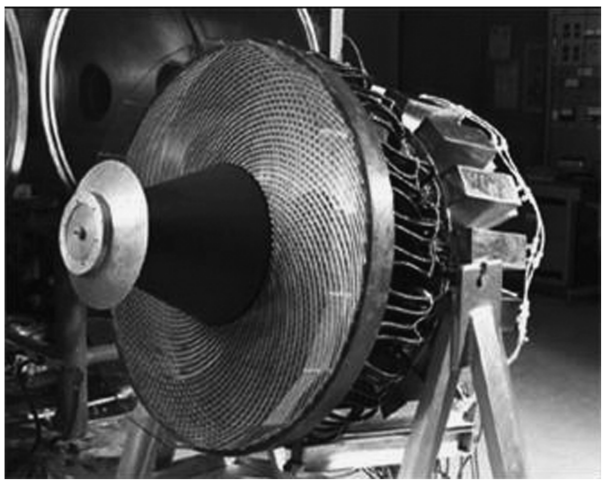

Fig. 12 Photograph of the PIT MK V (from [8]).

efficiently entrain and accelerate propellant. The strategy to increase the rise rate in the MK V was to both minimize the parasitic inductance of the thruster and substantially increase the azimuthal voltage applied to the acceleration coil.

The 1-m-diam coil used in the MK V was configured as parallel sets of windings forming a Marx-generator coil topology. One complete loop of this winding configuration is illustrated schematically in Fig. 13a. Two capacitors are connected in series by two half-turn spiral conductors formed from Litz wire. To keep the induced magnetic field uniform over the face of the coil, the conductors spiral radially inward on the front face of the accelerating coil over their first quarter-turn, and they spiral radially outward over the second quarter-turn. This configuration yields an azimuthal voltage drop around a complete loop equal to twice the charging voltage on each capacitor; that is, charging the capacitors to V_0 results in a total azimuthal voltage drop of $2V_0$. In the MK V, the Marx-generator configuration shown in Fig. 13a is offset 20 deg and replicated nine times to yield the coil shown in Fig. 13b. This configuration also reduces the parasitic inductance, because all the conductors to and from the individual capacitors are in parallel. The circuit had a total inductance of 740 nH, out of which approximately 60 nH was attributed to parasitic inductance. An additional issue resolved in the MK V design was the simultaneous triggering of multiple, independent spark-gap switches. A master pulse generator was employed, with transmission lines of equal length connecting it to every spark-gap switch; synchronicity was achieved by varying the pressure in each gap. Pulsed gas injection through a conical nozzle was used in all cases to feed propellant to the thruster.

Two versions of the thruster were tested. The first, officially designated the PIT MK V, had a total capacitance of 4.5 μF and a nominal energy of roughly 2 kJ/pulse at a capacitor charging voltage

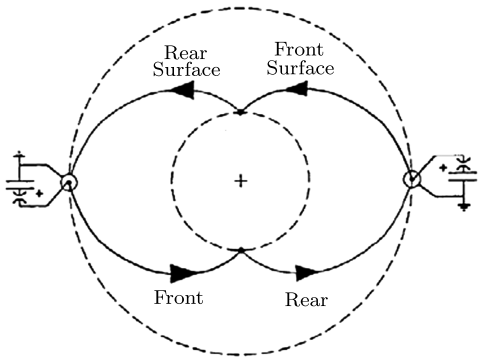

a)

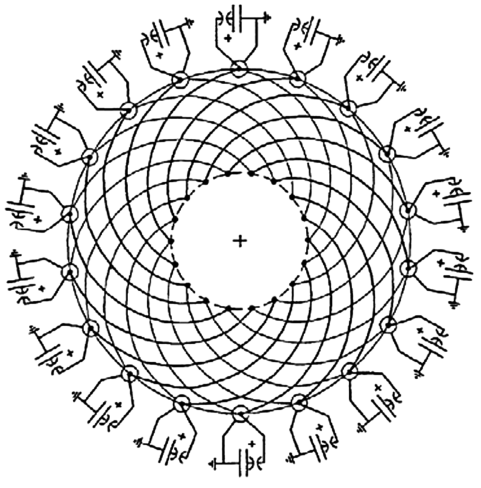

b)

Fig. 13 PIT MK V Marx-generator coil configuration: a) one complete Marx-generator loop and b) the nine complete loops comprising the PIT MK V (from [7]).

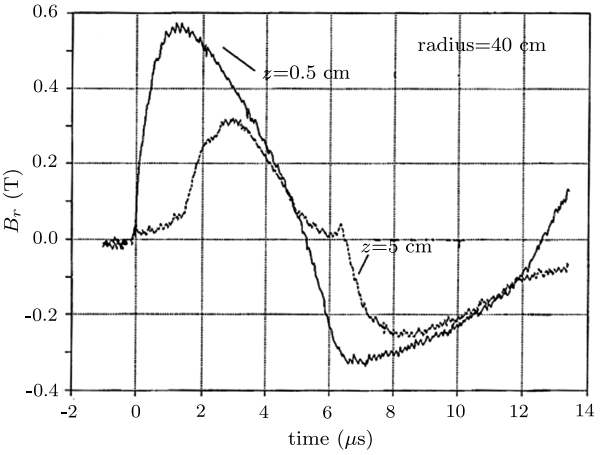

Fig. 14 Radial magnetic field measurements in the PIT MK Va at two axial locations (from [7]).

of 15 kV, yielding a total azimuthal voltage drop of 30 kV across the windings. The second version, the MK Va, had a total capacitance of 9 μF and a nominal energy of 4 kJ/pulse, with a capacitor charging voltage of 15 kV. As a clarifying point, the MK Va, which had the best performance and represents the current state of the art for PIT technology, is often referred to in the literature as the MK V. While performance of the MK Va (and to a lesser extent, the MK V) was extensively characterized using thrust balance measurements, it is the MK Va data that are typically cited. While it was noted that the sidewalls of the 1.2-m-diam metallic vacuum chamber could have affected the performance measurements, recent simulations have shown that the chamber wall does not have a large effect on performance [24,25].

1. *Performance Measurements*

Radial magnetic field waveforms from MK Va testing obtained at two axial locations are presented in Fig. 14. A comparison with the MK I data in Fig. 11a shows similarities associated with current-sheet formation and acceleration during the first half-cycle (asymmetric $z = 0.5$ cm waveform, delay before fast rise in downstream waveform). The magnetic field in the MK Va reaches a higher value than in the MK I, implying an improvement in performance. Indications of a second current sheet are observed in the magnetic field trace during the second half-cycle of the MK Va discharge, passing the $z = 5$ cm location at approximately 6.5 μs. The measurement at $z = 0.5$ cm is additionally useful, because it matches in form the waveform of the current flowing in the acceleration coil.

Performance data* (I_{sp} and η as functions of specific energy, defined as the ratio of the initial charge energy to the mass bit) from the MK V are shown for operation with ammonia and simulated hydrazine propellants in Fig. 15a and 15b and for argon, CO_2, and helium propellants in Figs. 15c and 15d. The simulated hydrazine propellant was injected as a mixture of dissociation products ($N_2 + 4NH_3$). We observe that data for a fixed specific energy have some spread, with the greater I_{sp} values typically corresponding to higher efficiencies. For all propellants, the specific impulse increases with specific energy, while the efficiency increases with specific energy for testing with ammonia, but it is relatively constant for almost every other propellant option. This trend is somewhat obfuscated by the data scatter at any particular specific energy. In a departure from the trends, the scaling of efficiency with specific energy for He propellant at 1296 J (12 kV charge voltage) is actually reversed. The generally low performance of the MK V was thought to be the result of the considerable difficulty associated with forming a consistent, impermeable current sheet at low discharge energies.* While the MK V thruster demonstrated the best performance with ammonia propellant followed by the simulated hydrazine, this was

*R. H. Lovberg, Private Communication, November 2001.

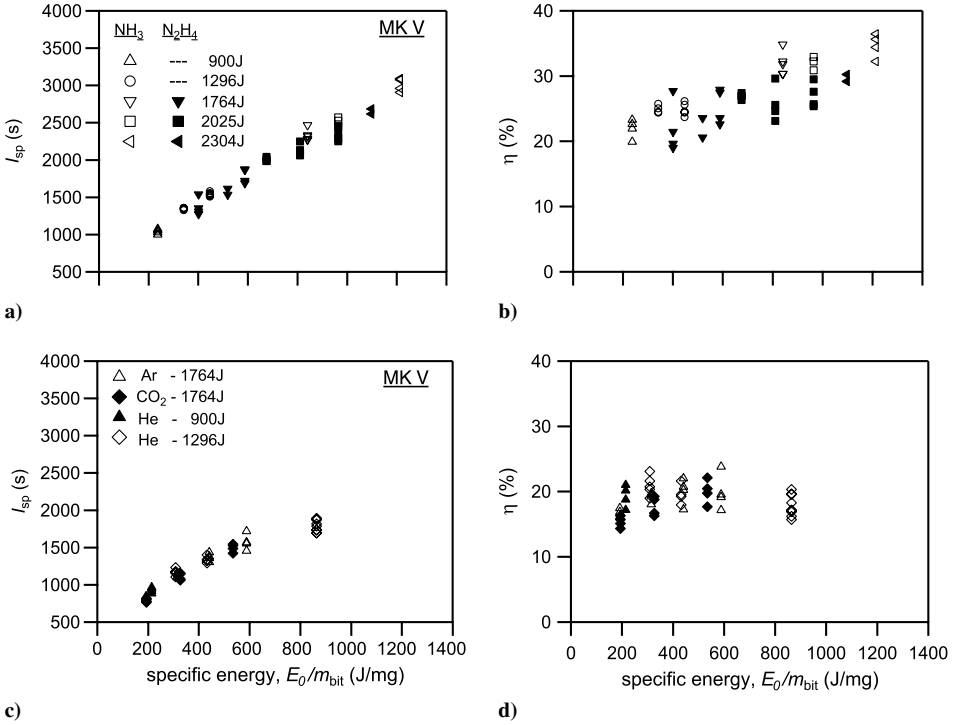

Fig. 15 Performance of the PIT MK V thruster operating on various propellants (see footnote *).

not a significant improvement over the MK I thruster performance (Fig. 10).

Data for the MK Va configuration operated on ammonia, and simulated hydrazine propellants [7] are presented in Figs. 16a–16d, respectively. Previous data indicated that these options showed promise for increasing thruster efficiency and, in fact, the MK Va thruster achieved performance levels that were greater than both the MK V and the earlier MK I thrusters, with I_{sp} again increasing with specific energy and thrust efficiency for ammonia exceeding 50%. In addition, the efficiency at the higher energies (greater than 4 kJ/pulse) is relatively constant over the range of specific energies tested. The improved performance of the MK Va compared with prior versions of the thruster reinforces the conclusion that high dI/dt levels in a PIT promote the breakdown process and lead to more efficient operation. Below 4 kJ/pulse, the efficiency decreases significantly with increasing specific energy, with reductions becoming more precipitous as the discharge energy is further lowered. As in the MK V, this reduction in efficiency was accompanied by incomplete propellant ionization and the formation of a nonuniform, magnetically permeable current sheet [7] (see footnote *).

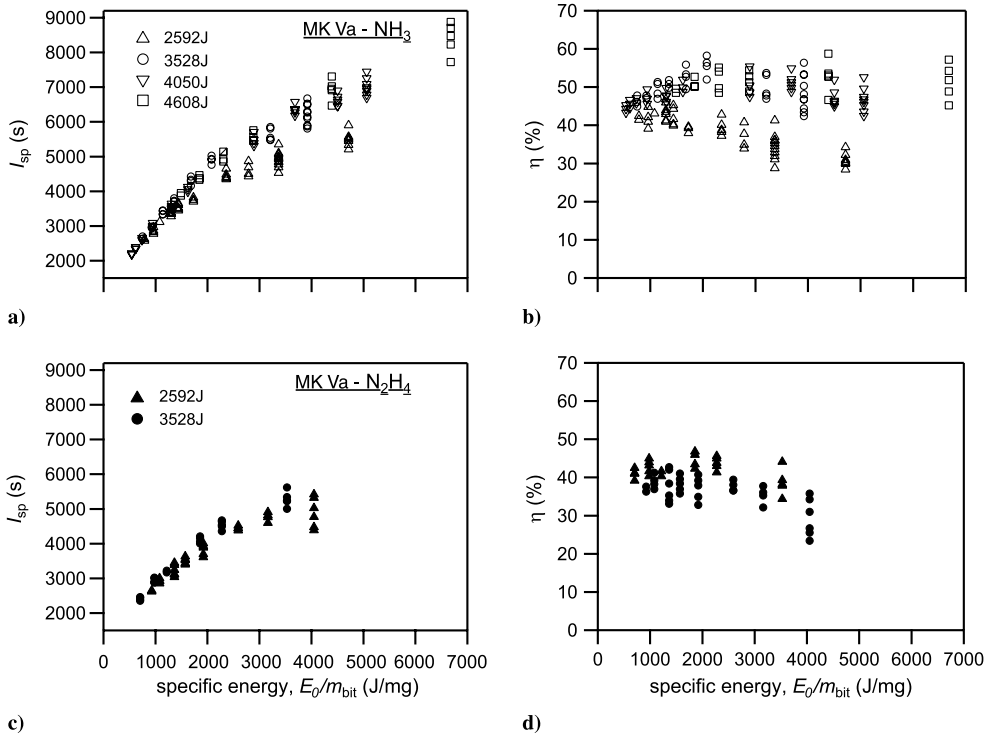

Fig. 16 Performance of the PIT MK Va thruster operating on ammonia and hydrazine propellants (from [7]).

The maximum value of η achieved in the MK Va thruster was explained as a consequence of matching the plasma acceleration timescale with the electrical period of the external circuit, which is generally predicted by the 1-D model discussed earlier. The manner by which this matching could be achieved was quantitatively addressed by an ad hoc set of rules derived from the MK Va design and aimed at providing guidance in selecting the values of circuit parameters for future thruster designs [8], but no attempt was made at that time to extend these empirical observations into a more universal set of rules applicable to the general class of pulsed inductive accelerators. The model also predicted that the efficiency could remain relatively constant in certain operating regimes over a broad range of I_{sp}, as observed in the higher discharge energy data from the MK Va, but the mechanism by which this occurred remained an open question. Finally, for the combination of lower mass bit and lower discharge energy, the data exhibited decreasing efficiency as specific energy increases. The physical origins of this trend were not well understood.

2. Summary of Important Results

The development of the PIT MK V and MK Va produced the following important results:

1) The MK Va thruster, using a Marx-generator coil geometry to increase the initial dI/dt in the coil and operating at approximately 4 kJ/pulse, presently represents the best-performing inductive thruster ever tested.

2) Relatively poor performance of the MK V resulted in a design change, with the resulting MK Va possessing a bank capacitance and discharge energy per pulse that was increased by a factor of two.

3) The best performance in the MK Va was observed with NH_3 propellant, with efficiencies exceeding 50%.

4) The peak in thruster efficiency was generally understood in terms of matching electrical and acceleration timescales, but it was not fully explained in terms of scaling with various controllable parameters.

5) High efficiency over a broad range of I_{sp} was observed in the high discharge energy NH_3 data and predicted by the 1-D model, but it was also not fully explained in this work.

6) For the combination of lower discharge energy and lower mass bit, the efficiency decreased dramatically with increasing specific energy. The physical origins of this observed trend were not well understood.

III. Recent Experimental Research and Development

Recently, several groups have pursued various parallel lines of planar PIT research and development. New experimental efforts seek to advance the state of the art of inductive thruster technology, either by making incremental improvements to various components and subsystems of an existing thruster or by implementing completely new designs that address deficiencies in the performance and/or lifetime of current state-of-the-art systems. These efforts are reviewed in this section.

A. Pulsed Inductive Thruster: 1993–Present

The MK Va thruster's high performance encouraged the TRW team to continue experimental efforts using that general design as their template. Newer iterations of the thruster would be similar to the MK Va, and they would be upgraded over time as new components and subsystems were developed to address various technical issues [26,27]. It was recognized that the spark-gap switches used in the MK Va would erode over time, and that increased lifetime could only be realized if these were replaced with high-current high-voltage solid-state switches. The high energy per pulse required by the PIT applied stringent constraints on the switch selection process. For high-power electric propulsion missions, a pulsed thruster needs to operate at a relatively high pulse rate (greater than 25 Hz at 100 kW_e) and deliver up to 10^{10} pulses [28]. In addition, the thruster must be able to endure the greater heat loads associated with high repetition-rate operation.

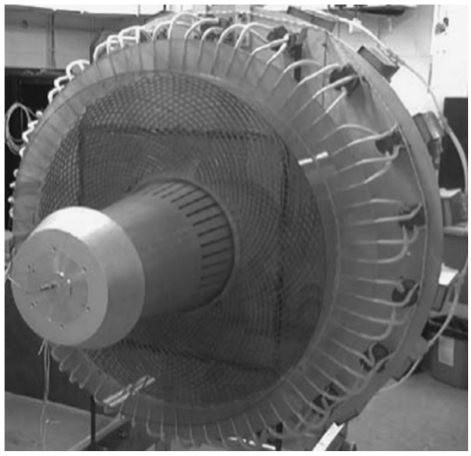

Fig. 17 Photograph of the PIT MK VI (from [30]).

The 300 kg PIT Mark VI [29,30], shown in Fig. 17, possessed a 1-m-diam acceleration coil that was configured in the same Marx-generator topology as the MK V. However, instead of Litz wire, this coil was formed from hollow copper tubing, which would enable the passing of coolant through the coil during high pulse rate operation. The capacitors and spark-gap switches were the same type used in the MK V. It was reported [30] that current traces for the MK VI indicated electrical properties that were very close to those of the MK V, with a total thruster inductance of 740 nH. A taller gas injection pylon was used for the MK VI, as this was predicted to yield a more even gas distribution over the coil face.

The MK VI did not adequately ionize the propellant or produce sufficient plasma current during the first half-cycle of the discharge to attain high performance [30]. Operation with a charging voltage of 15 kV (4050 J) and a mass bit of 2 mg ammonia resulted in a thrust efficiency of only 18.9% with an I_{sp} of 2750 s. This was well below the 50% efficiency and 5000 s specific impulse obtained in the MK Va with similar operating parameters. After testing, a fault was discovered in one of the spark-gap trigger units, which could have caused the thruster to underperform. Presently, no additional data on the MK VI are available in the literature to support this hypothesis.

Precursor hardware work for the Mark VII [29] primarily focused on the evaluation of commercial solid-state switches to determine if they could hold off a voltage of 15 kV, conduct a peak current of 13 kA, and permit a maximum current rise rate of 20 kA/μs. Two types of solid-state switches were tested. The first were standard thyristors, or silicon-controlled rectifiers (SCRs), which turn on when current is applied to the gate and turn off with the reversal of the load current. To accommodate the current and voltage hold-off requirements, a stack of five thyristors (Fig. 18) was used. The second type of switches tested were gate communicated thyristors (GCTs), which differ from SCRs in that they are turned on and turned off through the gate current.

The solid-state switch testing produced the following results. Near simultaneous switching of all five SCRs in the stack was achieved, which allowed the switching of a capacitor charged to 15 kV. A current waveform from this test is displayed in Fig. 19, and it reveals that the stacked SCRs conducted a peak current of 21 kA and achieved a maximum current rise rate of 27 kA/μs, exceeding the target requirements. Testing with the GCTs did not produce a successful result, as turnoff was not achieved at the end of either the first or second half-cycle of the discharge.

The most recent work on the PIT was consolidated under Northrop Grumman Space Technology's Nuclear-Electric PIT (NUPIT) program, which aimed at developing the MK VII thruster for high-power (200 kW_e) nuclear-electric propulsion missions [31]. The NUPIT program led to additional testing of solid-state switch technologies [32]. Again, both SCR and GCT switches were evaluated. The SCR effort quickly ended when the devices failed after only a few pulses. As in the previous testing, turnoff of the GCT switches was not achieved at the end of the first or second half-cycles.

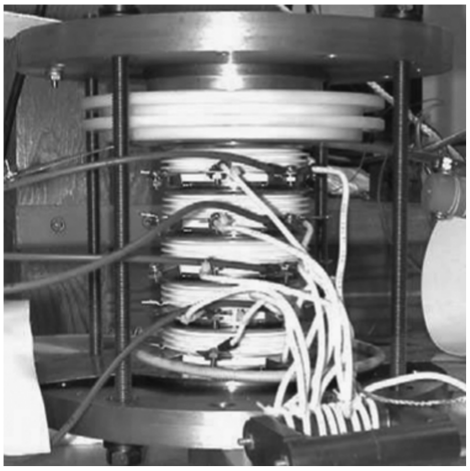

Fig. 18 Photograph of a clamped five-thyristor stack (from [29]).

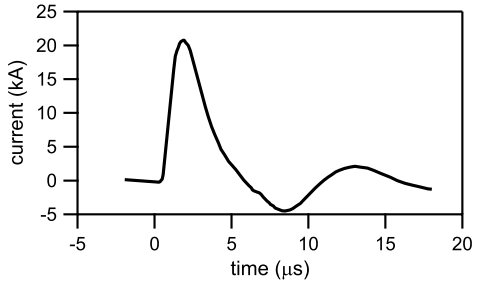

Fig. 19 Current waveform in a five-thyristor stack (from [29]).

Turnoff at the beginning of the third half-cycle of the discharge was demonstrated but only at current levels that were one-third to one-half of those encountered during full PIT operation. These devices failed relatively quickly due to a combination of excessive gate turnoff current and nonuniform clamping. It was believed, although not demonstrated, that with larger GCT devices, turnoff of the full PIT current load could be achieved before the third half-cycle of the discharge.

B. Faraday Accelerator with Radio-Frequency-Assisted Discharge

In 2004, the Faraday accelerator with radio-frequency assisted discharge (FARAD) was introduced [33]. The FARAD uses a pulsed current in a coil to induce a current in the plasma, accelerating the propellant in much the same manner as the PIT. Unlike the PIT, in which the propellant is both ionized and accelerated by the current pulse through the inductive coil, FARAD uses a separate preionization mechanism to form an inductive current sheet at much lower discharge energies and voltages.

Proof-of-concept experiments were performed at Princeton University, using the apparatus shown schematically in Fig. 20, to demonstrate the main operating features of FARAD and gain insight into the operation of this type of device [2,34]. Two cylindrical glass tubes were joined to form a vacuum chamber, with plasma generation occurring in the smaller vessel and acceleration taking place in the adjoining larger vessel. The assembled vacuum chamber is surrounded by a set of electromagnet coils, which were configured to produce a highly axial magnetic field inside the smaller tube and a highly diverging, mostly radial, magnetic field near the flat back end of the larger vacuum chamber, as shown by the representative B-field lines drawn in the figure. Gas was ionized by an inductive RF/helicon discharge and then guided by the applied magnetic field to flow radially outward along the flat back end of the adjoining larger chamber. An inductive coil was mounted just outside the entrance to the larger chamber and covered by an insulator to protect it from the plasma. The coil, which extends from the outer radius of the central

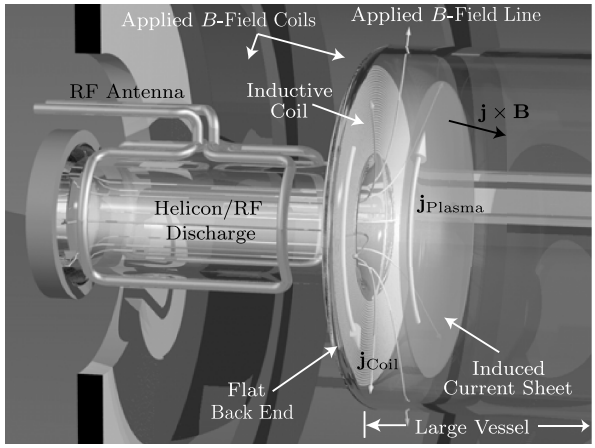

Fig. 20 Schematic illustration of the original FARAD concept (from [2]).

opening to the inner radius of the larger vessel, conducts a current pulse that accelerates the preionized propellant in much the same manner as the PIT. The coil is similar to, but smaller than, the Marx-type coil used in the PIT, possessing 12 half-turn coils with an inner diameter of 6 cm and an outer diameter of 20 cm. The coils were connected in parallel with a 39.2 μF capacitor.

The FARAD device was operated at a number of different conditions, but it was primarily studied using an ambient argon gas fill of 23 mtorr and a discharge energy of 78.5 J/pulse (2 kV charge voltage). A typical current measured in the induction coil for this operating condition is presented in Fig. 21, while measurements of the induced radial magnetic field obtained at various axial locations are presented in Fig. 22. In the induced magnetic field measurements (Fig. 22), the knee, or inflection point, in the data indicates current-sheet formation evidenced by associated increases in plasma conductivity and electromagnetic shielding. These data show that, at a relatively low discharge energy (compared with the 4 kJ/pulse PIT), a current sheet will form and translate axially during the pulse. The data also show a delay between initiation of current flow in the coil ($t = 0$) and formation of the current sheet.

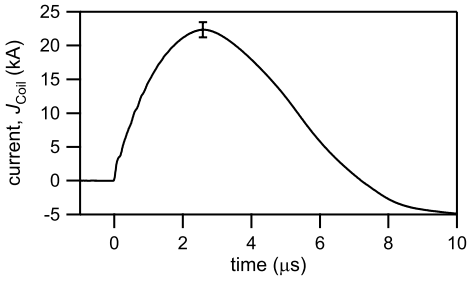

Fig. 21 Total current in the acceleration coil J_{Coil} (with a typical error bar) in the FARAD proof-of-concept experiment at a discharge energy of 78.5 J (from [2]).

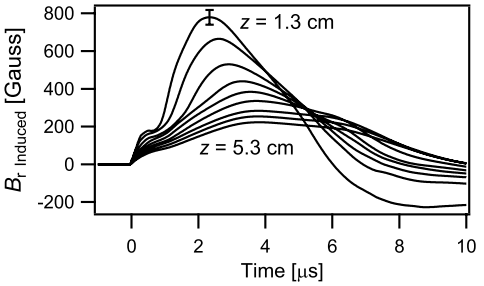

Fig. 22 Radial magnetic field in FARAD proof of concept at 78.5 J, 23 mtorr Ar backfill, $r = 66$ mm, z spaced evenly every 6 mm (from [2]).

The initial proof-of-concept experiments demonstrated that a preionized plasma allowed current-sheet formation and acceleration at lower discharge voltages and energies (down to 44 J/pulse) than in previous PIT designs [2,34]. It was further found that current-sheet formation at these low discharge energies was not possible without the preionization source. In addition, the applied magnetic field was required to properly direct plasma onto the acceleration coil face, as operation with the RF source but without the magnetic field failed to result in current-sheet formation.

One issue that arose in the initial experiments was the low fractional change in circuit inductance due to plasma motion found in the FARAD proof-of-concept setup [34]. In an efficient pulsed electromagnetic accelerator, this fraction, referred to as the Lovberg criteria, should be significantly greater than unity, as it is a measure of a thruster's ability to electromagnetically accelerate a gas [35]. Adopting the Marx-type coil geometry, which possesses a low inductance at small diameters, led to a fractional inductance change in the FARAD experiment of only 15%. A second issue in this testing was the significant stray inductance in the pulse circuit, which limited the current rise rate in the coil, leading to a delay in current-sheet formation. Finally, the neutral backfill gas exerted drag on the current sheet immediately after it began to accelerate. Consequently, the low coil inductance produced a current sheet that was not highly accelerated, and the current-sheet velocity was severely restricted by the neutral drag force [34]. Despite these issues, the experiment successfully demonstrated that using a separate preionization mechanism allowed the formation and acceleration of an inductive current sheet at much lower discharge energies and voltages than those previously used in the PIT. That this was demonstrated even in the highly unoptimized FARAD proof-of-concept configuration points to the potential utility of the concept, and the results inspired the generation of some new theoretical and experimental scaling relations and design rules [36,37], some of which are further discussed in the Sec. IV.

In more recent fundamental physics investigations on FARAD, the flat spiral coil has been traded for a conical theta pinch [38,39]. These studies have focused on plasma breakdown conditions (specifically, the inductive coupling of energy from the pinch coil into a gas that is already partially ionized) and have found that breakdown is dependent on the ratio of the induced electric field to the neutral gas background pressure. The FARAD conical theta-pinch coil is similar to the multiturn coil used on later versions of a conical theta-pinch field plasmoid thruster [3]; however, the FARAD conical theta pinch is meant to use current-sheet implosion (pinching) for plasma acceleration, while the plasmoid thruster is designed to form a compact toroid. Additional investigations with the FARAD thruster have traded the steady-state helicon/RF preionization method in one case (shown in Fig. 23) for a pulsed RF preionization discharge over a flat coil [40–42] using a vector inversion generator (VIG) [43,44] and, in another case, a steady-state microwave driven discharge in a conical theta-pinch geometry [45]. Presently, there are no additional performance data from any of these studies.

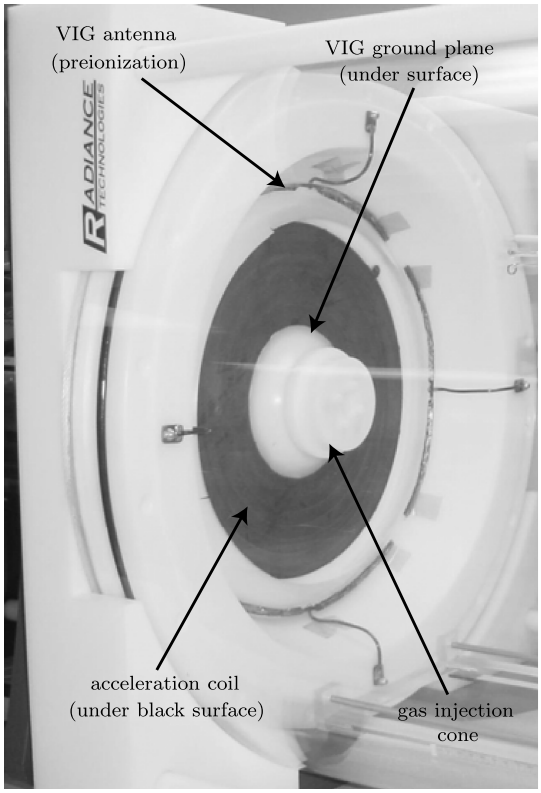

Fig. 23 Photograph of the FARAD laboratory-model thruster coupled to a vacuum chamber (from [41]).

C. Pulsed Power Trains for Inductive Thrusters

The circuit for the inductive acceleration coil of a PIT must be designed such that it can form a magnetically impermeable current sheet and then accelerate it efficiently. It must additionally handle the rigors of high-current switching over many pulses. As previously discussed, the switches must be capable of holding off $\mathcal{O}(1000\ \text{V})$ while switching at least $\mathcal{O}(10\ \text{kA})$ of current, and the jitter must be $\mathcal{O}(10\ \text{ns})$ if multiple switches are to be simultaneously triggered. Solid-state switching in PITs is most difficult in the case where there is no propellant preionization. The switches must not only meet the voltage, current, and rise rate requirements for current-sheet formation, but their integration into the pulse circuit must not introduce additional stray inductance that would reduce the current rise rate. These issues are somewhat mitigated by employing preionization, as used in FARAD [2,34,40], which reduces the switching requirements and makes the application of current solid-state components possible. To approach the lifetime and total deliverable impulse provided by other, competing electric propulsion systems, both the higher energy-per-pulse nonpreionized option and the lower energy-per-pulse options must be capable of operating for at least 10^9–10^{10} pulses [28,46].

In the remainder of this section, we review several different pulsed power trains and circuit topologies that could be used in a PIT and note how each can potentially address and mitigate many of the issues listed previously.

1. *Simple RLC Circuit Topology*

The PIT, in both the single capacitor bank and Marx-generator configurations, can be electrically represented by an equivalent lumped-element *RLC* circuit topology (as shown in Fig. 7), which is the base to which other power trains discussed in this section will be compared. The topology of the MK V and MK Va allowed for low parasitic inductance and an initial charge voltage equal to twice the voltage applied to a single capacitor. Both of these factors led to an increase in the current rise rate, relative to previous versions of the PIT [37]. However, the discharge voltage and current rise rate requirements are high in the PIT, since it operates without preionization. In either the single capacitor bank or Marx-generator configurations, solid-state components cannot presently meet the switching requirements for efficient PIT operation; hence, life-limited spark-gap switches have been employed. In the Marx-generator configuration, there is an additional difficulty in that the individual switches (either solid state or spark gap) on each capacitor must be triggered simultaneously for effective operation.

2. *Pulse Compressor Power Train*

An alternative power train that enables the use of solid-state switching is a pulse compressor [47], shown in Fig. 24 and illustrated schematically in Fig. 25. In this approach, an initially slow low-current pulse that can be switched using current solid-state switching technology originates from capacitor C_1 and progresses through a series of resonant transfer stages that transform the waveform into a time-compressed high-current pulse [40,47,48]. While a multistage pulse compressor may be more massive than other systems, it can

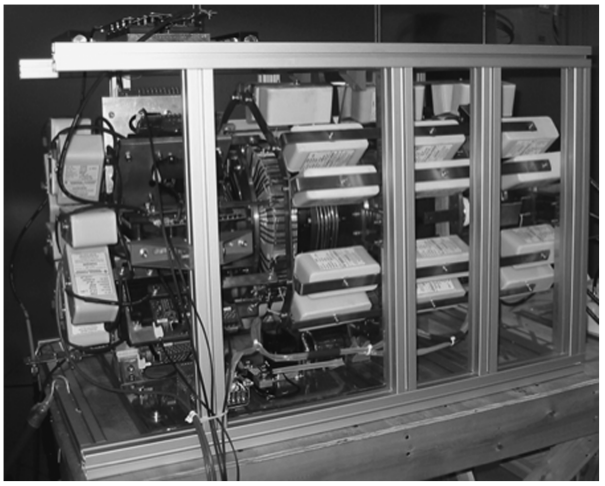

Fig. 24 Photograph of a 100 J pulse compression ring powertrain (from [47]).

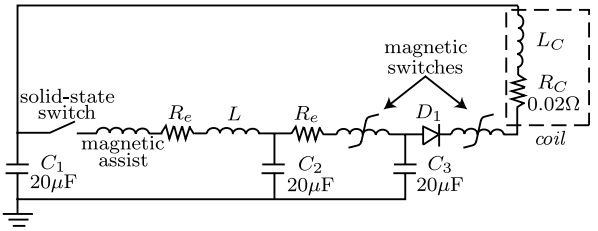

Fig. 25 Electrical schematic model of a pulse compression ring circuit (from [40]).

provide sufficient time compression to yield a pulse that can drive plasma acceleration in a PIT. The circuit depicted in Fig. 25 uses diodes D_1 to ensure that current can only flow through the coil in one direction, eliminating voltage reversal on the capacitors and helping to increase capacitor lifetime. Sample waveforms showing the current and capacitor voltages in the depicted pulse compressor circuit discharged into a constant inductive load are presented in Fig. 26.

3. *Bernardes and Merryman Power Train*

The Bernardes and Merryman (B–M) [49] pulsed power train, shown schematically in Fig. 27a, is a variation on a *RLC* circuit that possesses two capacitor banks of equal capacitance connected in series through the acceleration coil. Sample experimental waveforms showing the current and capacitor voltages from a B–M circuit discharged into a constant inductive load are presented in Fig. 27b. The data show that residual voltage remains on each capacitor after a pulse. A power train's ability to recapture this residual, unused energy and apply it to subsequent pulses can lead to increased electrical efficiency while helping to reduce the overall power system and radiator requirements, making PITs more attractive for certain missions. We observe that the topology also precludes voltage reversals on either capacitor, potentially reducing the operational stress and increasing component lifetimes. It should be noted that the separate circuit loops in the pulse compressor, shown in Fig. 25, also do not experience voltage reversals, since they are functionally similar to the B–M circuit topology.

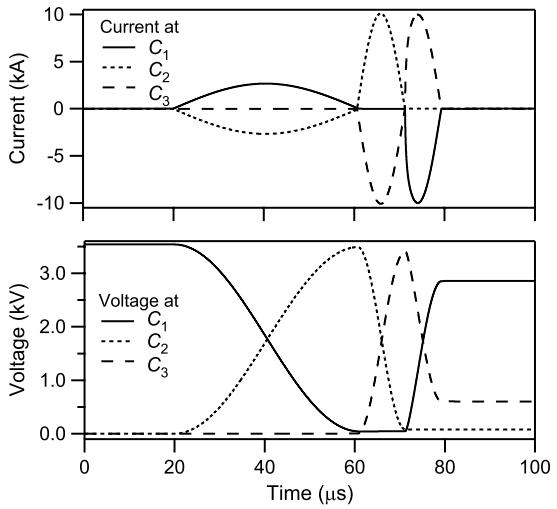

Fig. 26 Circuit simulation results giving current and voltage characteristics at each capacitor in a single-stage pulse compressor (from [40]).

The ability of the B–M circuit to recover energy may be further improved by employing a latching design [40]. This concept is illustrated schematically in Fig. 28a, where latching diodes have been added in parallel to the two switches: one for each capacitor bank. The diodes serve to reduce the amount of energy resistively dissipated in the discharge by allowing current to flow in the circuit for only the first half-cycle of the discharge. The initially uncharged capacitor bank is partially charged by the current flowing through the coil from C_1 to C_2 (Fig. 28b). This further reduces the amount of energy that must be expended relative to the unlatched B–M to fully charge C_2 before the next pulse.

4. *Summary of Important Results*

Experimental research and development efforts since 1993 have produced the following important results:

1) The PIT MK VI thruster failed to replicate the high performance results of the MK Va, potentially due to a fault in one of the thruster's spark-gap switches.

2) Testing of solid-state switching options at the current and voltage levels required by the PIT was relatively unsuccessful, with the switches failing relatively early in the test sequence.

3) The FARAD thruster was introduced, demonstrating that the use of a separate preionization mechanism in a PIT can dramatically lower the voltage and current thresholds required to inductively form and accelerate a current sheet.

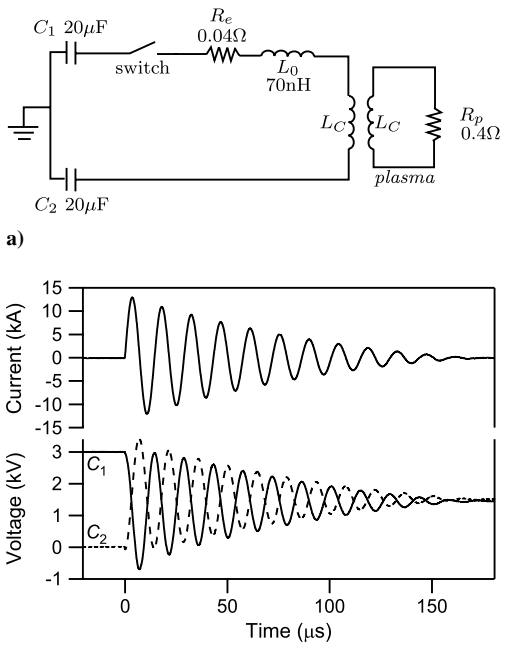

Fig. 27 B–M circuit: a) schematic and b) current and voltage waveforms for C_1 and C_2 discharging into a 540 nH load (from [40]).

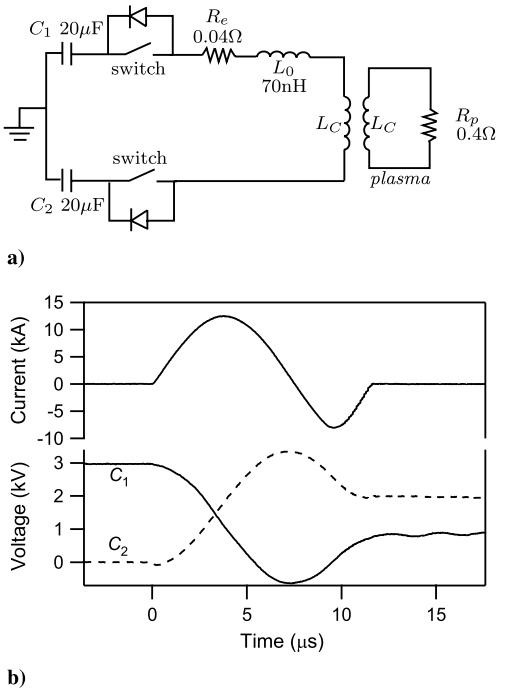

Fig. 28 Diode-latched B–M: a) schematic and b) current and voltage waveforms for C_1 and C_2 (from [40]).

4) Pulse-forming power train variants of the *RLC* circuit topology were investigated as options to either lower switching requirements (pulse compressor) or explicitly permit energy recovery (B–M).

IV. Recent Theoretical and Numerical Investigations

In parallel with experimental efforts, several recent modeling efforts have been undertaken that have resulted in an enhanced understanding of pulsed inductive accelerators. These efforts and their results and insights are reviewed in this section.

A. Pulsed Inductive Thruster Simulation and Modeling

Since 2002, Mikellides [50,51] has been refining numerical simulations of the PIT (specifically, the MK V and MK Va) to accurately capture its performance while simultaneously developing models to provide additional physical insights into thruster operation.

1. Magnetohydrodynamic Numerical Modeling

Numerical modeling of the PIT has been performed using the 2-D axisymmetric multiblock arbitrary coordinate hydromagnetic (MACH) code, which is capable of capturing the time-dependent evolution of the plasma. Real gas equations of state are used, including a thermal nonequilibrium equation of state for ammonia that was developed during the course of the modeling effort [52]. Use of the MACH code served a dual purpose in validating the ability to model the geometry and internal physical processes of the PIT while simultaneously capturing the performance of the thruster and extracting insight regarding operation [53].

Much of the plasma modeling was performed using a generic magnetic field boundary condition that did not couple the external circuit response to the plasma dynamics associated with the accelerating current sheet [53,54]. The computed performance of the PIT MK V operating below 2 kJ/pulse on He, Ar, and NH_3 is compared with experimental data (exhaust velocity as a function of specific energy) in Figs. 29a–29c, respectively. These data show that, in this operating regime, the computed performance agrees very well with the experimental data without any coupling of the circuit response to the plasma dynamics.

Simulations of the MK Va using the uncoupled circuit equation underestimated thruster performance. This implied a more efficient

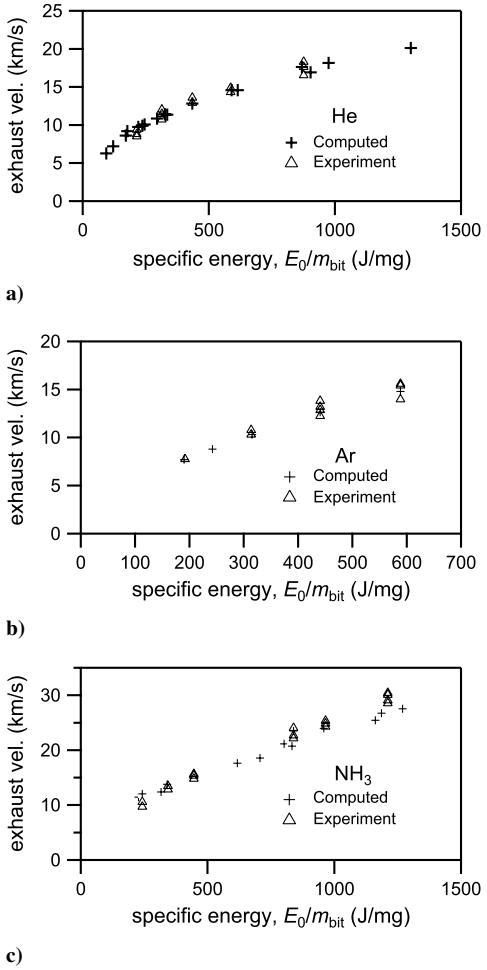

Fig. 29 Computed and measured exhaust velocities: a) He, b) Ar, and c) NH_3 (from [54]).

coupling of the plasma and field at the higher discharge energies tested in the MK Va, owing to a more significant contribution of the time-varying inductance $\dot{L}$ to acceleration. These results motivated the development of a coupled circuit model formulation [55]. The model is based on the circuit given in Fig. 30, where the plasma dynamics is contained in the time-varying plasma voltage $V_p(t)$. The circuit behavior is governed by the differential equation

$$V(t) - L_0\dot{I}(t) - R_e I(t) - V_p(t) = 0 \tag{6}$$

where the plasma voltage is given by

$$V_p(t) = R_p(t)I(t) + \dot{\phi}(t) = L_p(t)\dot{I}(t) + [R_p(t) + \dot{L}_p(t)]I(t) \tag{7}$$

The magnetic flux, commensurate plasma inductance L_p, and ohmic heating in the plasma are readily computed at each time step from the output of the MACH solver. Figure 31 provides a comparison of the experimental magnetic field waveform obtained in

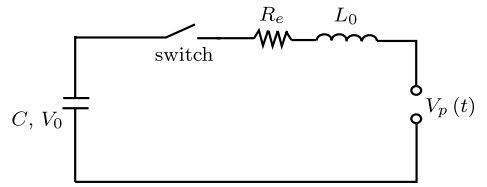

Fig. 30 Circuit schematic for an LRC circuit coupled to a dynamic current sheet (from [55]).

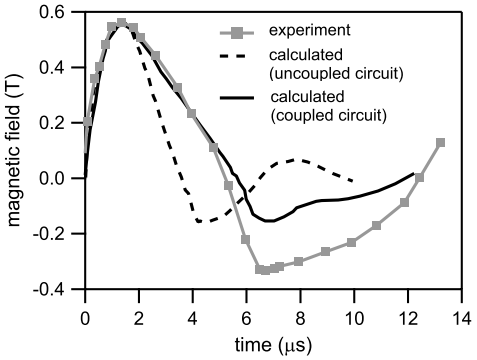

Fig. 31 MK Va experimental (from [7]) and computed magnetic field waveforms: uncoupled circuit (from [54]) and coupled circuit (from [55]).

the PIT MK Va at the axial position $z = 0.5$ cm with computed waveforms generated using both the uncoupled and coupled circuit models, with the coupled model exhibiting more favorable agreement throughout the first half-cycle of the pulse.

Performance data computed using the coupled circuit equation for the MK Va operating on ammonia propellant are presented and compared with experimental data sets in Fig. 32. The computed performance and the experimental data compare favorably for all three discharge energies. The trend of constant or decreasing efficiency is captured by the simulations, but there are discrepancies in the actual values computed, especially at the lower discharge energy levels. These discrepancies are thought to be mainly due to incomplete breakdown of the plasma in the experiments, leading to nonuniformities in the current sheet, which has historically resulted in lower than predicted performance.

2. Critical Mass Phenomenon

In the experimental data from the MK V and MK Va (specifically Figs. 15c, 15d, and 16), the efficiency at certain discharge energies drops precipitously for operation below a given propellant mass bit. This phenomenon was investigated using the MACH simulations [53]. Specifically, the code output was used to compute the fraction of energy ξ deposited into all the nonpropulsive modes. It was found for simulations of the MK V that, above a certain mass bit, the value of ξ was approximately constant for each propellant, regardless of the discharge energy. In addition, analytical performance modeling, where the problem was significantly simplified to yield additional insight into the problem, also yielded constant ξ for mass bits above a threshold value [53].

Below the critical mass bit, the fraction of energy directed into nonpropulsive modes increased rapidly. The threshold roughly corresponds to the critical mass m_c or critical specific energy e_0^*, given as [53]

$$\text{critical mass: } m_c = \frac{ME_0}{Q_1} \quad \text{or}$$

$$\text{critical specific energy: } e_0^* = \frac{E_0}{m_c} = \frac{Q_1}{M} \tag{8}$$

where M is the molecular mass, Q_1 is the first ionization potential and E_0 is the discharge energy. This threshold corresponds to the Alfvén critical ionization velocity that, in many plasma applications, is a limiting velocity where, instead of further accelerating the propellant, additional input energy is redirected into internal plasma modes until the propellant is fully singly ionized [56]. The critical specific energy for He is approximated quite well using just the first ionization level, resulting in $e_0^* = 593$ J/mg. Equation (8) can be modified to account for multiple ionization levels, resulting in $e_0^* > 10^4$ J/mg and $e_0^* = 1800$ J/mg for Ar and NH_3, respectively.

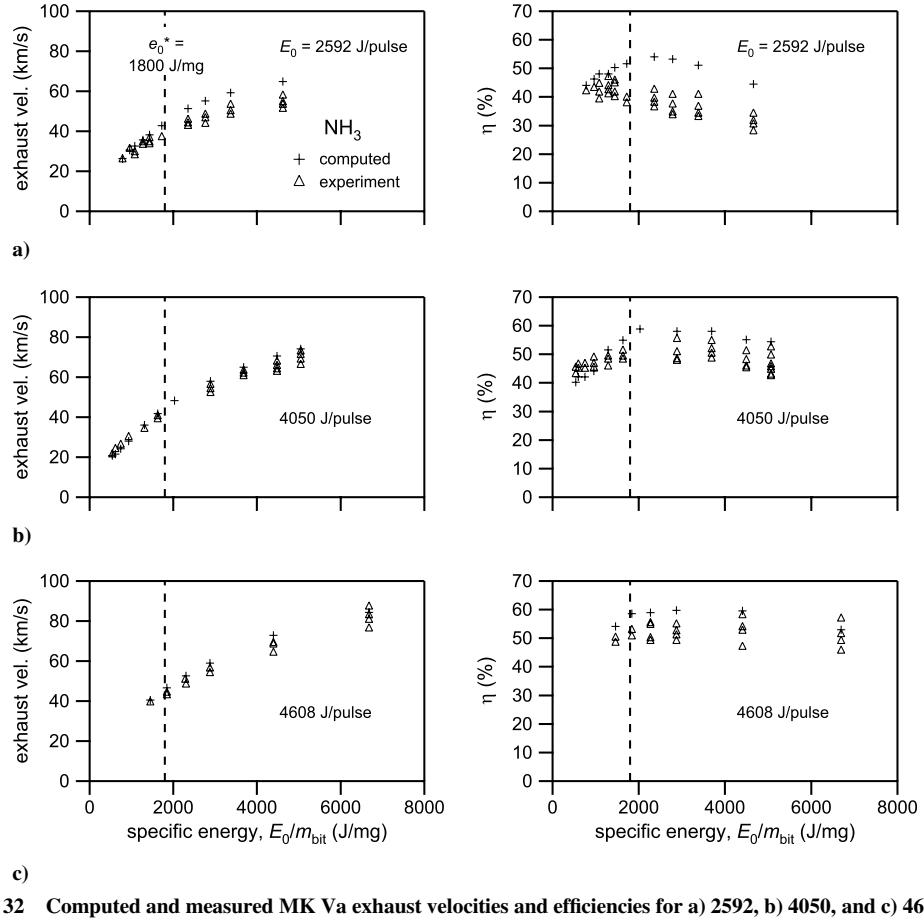

Fig. 32 Computed and measured MK Va exhaust velocities and efficiencies for a) 2592, b) 4050, and c) 4608 J.

The critical mass phenomenon is observed in the 1296 J/pulse He data [53] previously presented in Figs. 15c and 15d for the MK V. The very high value of e_0^* for Ar requires a very small mass bit and/or extremely high energy to cause the occurrence of the critical mass phenomenon, which is not observed in the MK V since neither extreme case for Ar was tested. The NH_3 data from the MK V in Figs. 15a and 15b do not exhibit a reduction in efficiency as the mass bit is reduced [53,54], but the data in Figs. 16a and 16b from the MK Va do exhibit such a trend [55], because the discharge energy and, consequently, the specific energy per pulse are greater than in the MK V.

3. *Insights into Performance on Ammonia*

Much of the investigation into the PIT MK V and MK Va has been inspired by the exceptionally high performance with NH_3, and the MACH simulations provide useful insight into this aspect of PIT performance. Simulations of the MK V operating on He and Ar were performed using a model for radiative plasma cooling [54], which was essential in attaining agreement with the data presented in Figs. 29a and 29b. At the time the MK V simulations were performed for NH_3, no radiation model for ammonia existed, and these losses were not included [54]. However, as shown in Fig. 29c, even without radiation losses, the model was able to accurately capture the performance of the thruster. This strongly implied that, unlike He and Ar, radiation losses were not important for ammonia [54]. This conclusion was further strengthened by higher energy simulations of the MK Va operated with NH_3, as shown in Fig. 32 where performance levels and trends were again accurately captured without the use of a radiative energy transfer model. The modeling resulted in the conclusion that the high efficiency obtained by operating with NH_3 is due mainly to a radiative energy sink that is small relative to that found in other tested propellants. While good agreement with modeling was obtained for both the MK V and MK Va, it should be noted that this does not necessarily mean that radiation will be unimportant at all other operating conditions and in different devices.

B. Inductive Thruster Performance Scaling

The thrust efficiency and specific impulse attained by a PIT are a function of the lumped-circuit values of the components comprising the acceleration stage. The first attempt to address this functional relationship was based on the results from testing with the PIT MK Va and was semiempirical in nature [8]. These original design rules were only applicable to thrusters that were similar to the MK V, both in size and geometry, presenting the scaling for various component values in a semiquantitative manner. Recently, the circuit-based performance model [34,36], previously reviewed in Sec. II.B.2 of this paper, was nondimensionalized to identify dimensionless scaling parameters that control the performance of pulsed inductive accelerators. While this work was performed assuming that the coil was connected in series to a capacitor forming a simple *RLC* circuit, a similar analysis could be performed assuming one of the other pulsed power drive train configurations.

1. *Scaling Parameters*

The relevant scaling parameters for a pulsed inductive plasma accelerator, which were previously presented in [34,36], are briefly reviewed next.

a. Inductance Ratio L^*. A pulsed inductive accelerator circuit possesses an external inductance L_0 and an acceleration coil inductance L_C, and during a current pulse, the moving plasma increases the circuit's inductance from L_0 to $L_0 + L_C$ (i.e., $L_C = \Delta L$). The fractional change of inductance, $(L^*)^{-1} = \Delta L/L_0$, in a pulsed electromagnetic accelerator provides a measure of efficiency [35], as this ratio is indicative of the fraction of energy that can be deposited into electromagnetic acceleration of the gas. Consequently, the value of L^* must be much less than unity or $L_C \gg L_0$ in an efficient pulsed inductive accelerator. Working separately and applying the same governing equation set to a conical theta-pinch geometry, Martin and Eskridge [57] arrived at the same conclusion regarding the desired value of L^*.

b. Critical Resistance Ratios ψ_1 and ψ_2. The critical resistance ratios are defined as

$$\psi_1 = R_e\sqrt{\frac{C}{L_0}} \qquad \psi_2 = R_p\sqrt{\frac{C}{L_0}} \tag{9}$$

These parameters (or more specifically, their average $\Psi \equiv (\psi_1 + \psi_2)/2$) control the nature of the current waveform in the acceleration coil: overdamped if $\Psi > 1$, critically damped for Ψ of unity, and underdamped (ringing) for $\Psi < 1$. It was found [36] that underdamped circuits are preferable for greater efficiency and exhaust velocity, yielding a current that peaks while the plasma is still close to the acceleration coil to provide maximum momentum transferred to the propellant.

c. Dynamic Impedance Parameter α. The dynamic impedance parameter α is similar to that found in the PPT literature [6] and can be written as the product of several important ratios:

$$\alpha = \frac{C^2V_0^2L_C}{2m_{\text{bit}}z_0^2} = \frac{1}{8\pi^2}\frac{CV_0^2/2}{m_{\text{bit}}v_z^2/2}L^*\left(\frac{2\pi\sqrt{L_0C}}{L_0/\dot{L}}\right)^2 \tag{10}$$

where $\dot{L}$ is the dynamic impedance, defined as v_zL', and L' is the effective inductance per unit length, equal to L_C/z_0. The ratio of the initial stored energy ($CV_0^2/2$) to the plasma kinetic energy ($m_{\text{bit}}v_z^2/2$) is recognized as the inverse of thrust efficiency η^{-1} and will always be greater than one. The final term is the ratio of the natural period of the external circuit, $2\pi\sqrt{L_0C}$, to the time interval, $L_0/\dot{L}$, over which the plasma's motion increases the inductance of the circuit by one unit of L_0. The former is the timescale on which the external circuit naturally operates, while the latter is the timescale on which the current sheet remains electromagnetically coupled to the acceleration coil.

For a given configuration, there exists an optimum value of α (see Fig. 33) where the electromagnetic coupling timescale is matched to the frequency of the external circuit, allowing for optimum transfer of stored electrical energy into directed kinetic energy. Solutions to the coupled circuit and momentum equations governing PIT operation show an optimum α near three for mass distributions like those found in the PIT MK V and MK Va [36].

2. *Nondimensional Study Results*

The system of nondimensional equations [36] was solved by varying the values of different scaling parameters to learn the effect each had on accelerator performance. This exercise led to several important and insightful conclusions that are summarized next.

a. Propellant Distribution. An inductively driven current sheet propagating into propellant with substantial velocity experiences significant drag (drag force $\propto v_z^2$) while at the same time the driving force applied to the current sheet by the coil decreases exponentially with increasing axial position. As a consequence, the thrust efficiency can be high for a slug mass loading, but for a uniform propellant loading where the current sheet propagates into a gas of constant density, the efficiency drops precipitously due to large mass entrainment losses [36]. The mass loading in the PIT was triangular, with a maximum density at the coil face and a linear decrease to zero over some finite distance. This was the distribution used in the generation of Fig. 33.

b. Comparison of Computed and Experimental Performance. Contours of constant thrust efficiency for the PIT MK Va as a function of α and ψ_1 (for fixed $\psi_2 = 0.13$ and $L^* = 0.121$) are presented in Fig. 33a. In addition, simulation results showing the efficiency as a function of α for the MK V ($\psi_1 = 0.035$, $\psi_2 = 0.09$, and $L^* = 0.121$) and MK Va ($\psi_1 = 0.05$, $\psi_2 = 0.13$, and $L^* = 0.121$) are plotted in Fig. 33b. These simulation results are compared with experimental data from both thrusters operating on ammonia propellant [7] (see footnote *). The experimental data compare quite favorably, both qualitatively and quantitatively, with the computed performance. The lower capacitance places the MK V experimental data all to one side of the local maximum in thrust

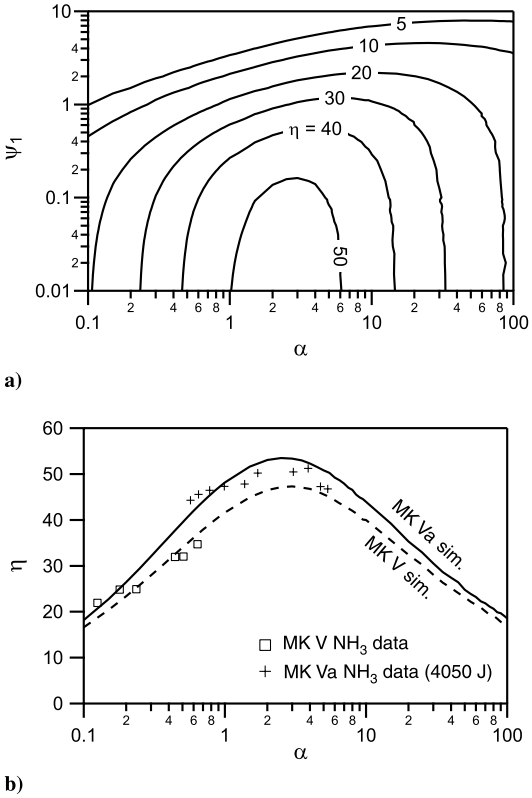

Fig. 33 Computed PIT efficiencies: a) contours for the MK Va and b) comparisons with MK V and MK Va performance data (after [7]).

efficiency, while the MK Va data span the local maximum in efficiency where the impedance match between the electrical circuit and the plasma load is optimum.

C. Overlaps in Performance Modeling Efforts

There are instances in the work reviewed where the full magnetohydrodynamics (MHD) simulations and the dimensionless performance modeling, when taken together, provide a more complete picture of pulsed inductive accelerator physics. Two examples of this are given next.

1. ξ, α, and Thruster Performance

The MHD modeling generally captures the performance trends measured in the MK V and MK Va thrusters, and the nondimensional simulations accurately model the performance of these thrusters operating on NH_3, where radiation losses are not important. The MHD modeling shows that, above the critical mass limit, the value of ξ, which is representative of the amount of energy directed into nonpropulsive energy modes, possesses a constant value that is higher in the MK V than in the MK Va. The nondimensional modeling in Fig. 33b shows that the performance is generally greater in the MK Va due to a better dynamic impedance match between the electrical circuit and the plasma load. However, we also observe that, even if the MK V were operating at the optimum α, it would still underperform the MK Va because of the inherent electrodynamic limits on the amount of energy that can be directed into plasma kinetic energy. Both modeling efforts support the conclusion that, compared with the MK Va, the MK V possesses a greater value of ξ, leaving less energy available for propulsive modes.

2. High Performance of Mark Va on Ammonia

It was inferred from the MACH modeling of the PIT that radiation losses for operation with NH_3 were small and unimportant when compared with the radiation losses incurred using other propellants such as He and Ar. The dimensionless performance model lacks a governing equation for the energy distribution, so the results do not differentiate between various propellant species on the basis of internal and radiative energy sinks. However, both the MACH simulations performed without a radiation model and the dimensionless simulations show quantitative agreement with the performance values for NH_3. The dual success of these models further supports the supposition that the high performance with NH_3 is the result of a case where radiation energy losses are negligible. As noted earlier, this may not be a general result extendable to all other devices and operating conditions.

D. Thruster Design Rules

Lovberg and Dailey provided a set of PIT scaling guidelines in [8]. The scaling relations were a somewhat ad hoc set of rules based on the performance of a single thruster, the PIT MK Va. Their technique involved fixing certain design parameters and then calculating all the other parameters based on the scaling in the MK Va, iterating until the desired performance was achieved. These rules, while having solid heuristic arguments to support them, were not buttressed with detailed performance modeling of the thruster.

Work by Polzin [37,58] served to augment the performance scaling relations and provided additional guidelines for obtaining an inductively coupled, magnetically impermeable, current sheet. The prior ad hoc rules for thruster performance were replaced with the nondimensional scaling parameters presented in Sec. IV.B.1 of this paper. This scaling, which generally matched the set derived from MK Va data, was based on a rigorous numerical study where the effects of each nondimensional parameter on performance were quantified [36]. To address the issue of current-sheet formation, data from several thrusters were compared with place lower and upper bounds on the required current density rise rate in the inductive coil. Data from the MK I, MK IV, and MK Va were used to bound the rise rate in PITs that did not employ preionization, and data from the FARAD proof-of-concept experiment were added to find a lower bound for propellants that were preionized [37].

E. Summary of Important Results

Theoretical and numerical studies of PITs since 1993 have produced the following key results:

1) The MACH modeling of PIT generally matched experimental data showing a high efficiency over a broad range of specific impulse. A model that coupled the circuit response to the plasma dynamics was necessary to simulate the MK Va.

2) A mechanism similar to the Alfvén critical ionization velocity energy sink was suggested as the cause of the severe reduction in MK Va efficiency at lower mass bits.

3) Nondimensionalization of the 1-D acceleration model resulted in the discovery of several dimensionless scaling parameters that control performance and can be used in the design of thrusters.

4) For an *RLC* drive circuit, the model shows that an underdamped response is desired for increased efficiency.

5) Efficiency as a function of the dynamic impedance parameter has a maximum value where the acceleration and circuit response timescales are matched. The scaling agrees with the data from the MK V and MK Va.

6) MACH simulations and the dimensionless modeling suggest that high performance in the MK Va operating on NH_3 is due to the lack of a radiation energy sink.

V. Conclusions

Breakthrough work on planar pulsed inductive plasma accelerators was initially performed at TRW Space Systems, and those efforts, spanning nearly 30 years, produced a remarkable amount of data and many of the important physical insights that presently anchor the PIT knowledge base. These data, in conjunction with more recent experimental studies and detailed physical and numerical modeling efforts, continue to yield important additional insights into inductive thruster operation and performance scaling. Next is a summary of the major findings and insights that have been produced to date through PIT research and development:

1) The performance of a PIT was typically greatest when a uniform current sheet was produced. This was typically the result of a high-current rise rate (realized through a combination of high charge voltage and low initial inductance) and a uniform gas density over the coil face.

2) Larger diameter acceleration coils in the PIT allowed for a greater electromagnetic coupling distance, which in turn permitted greater efficiency.

3) Performance was maximized in the PIT MK I, MK V, and MK Va when operating on NH_3 propellant, with efficiency of approximately 50% over a broad range of specific impulse values in the MK Va.

4) An inductive preionization pulse through the acceleration coil of a pulsed inductive coil was not effective, proving to be detrimental to the overall performance.

5) Decoupling the preionization and inductive acceleration processes by using an alternative RF discharge permitted current-sheet formation at much lower voltages and discharge energies than in the PIT, where no preionization was employed.

6) Modeling suggests that the high performance on NH_3 is due to a lack of an appreciable radiation energy sink, compared with other propellants, at the discharge energies tested.

7) A critical ionization velocity energy sink has been proposed as the mechanism for the reduced performance observed in the MK Va data obtained at a low mass bit (or at specific energies greater than the critical specific energy).

8) Nondimensionalization of the acceleration model yielded dimensionless parameters, which were used to systematically explore accelerator performance scaling. Efficiency was increased for an underdamped electrical circuit response, and a maximum value of efficiency was found to correspond to the case where the acceleration and circuit response timescales were matched.

While the seminal and far-reaching work that eventually culminated in the PIT MK Va will continue to influence and guide PIT research and development efforts, the more recent approaches are currently driving additional improvements to the technology that should lead to more efficient, more robust thruster designs that could be applied to future missions.

Acknowledgments

The author is grateful to Michael LaPointe, who carefully reviewed the manuscript and suggested many corrections and changes that greatly improved the quality of the work. In addition, this effort has greatly benefited from helpful discussions over the past few years with many individuals, including Robert Jahn, Edgar Choueiri, Pavlos Mikellides, Frank Rose, Thomas Owens, Roger Myers, Robert Miller, and Steve Best. Finally, the author wishes to acknowledge continued NASA Marshall Space Flight Center management support from Jim Martin, J. Boise Pearson, and Sally Ann Little.

References

[1] Lovberg, R. H., and Dailey, C. L., "Large Inductive Thruster Performance Measurement," *AIAA Journal*, Vol. 20, No. 7, 1982, pp. 971–977. doi:10.2514/3.51155

[2] Choueiri, E. Y., and Polzin, K. A., "Faraday Acceleration with Radio-Frequency Assisted Discharge," *Journal of Propulsion and Power*, Vol. 22, No. 3, 2006, pp. 611–619. doi:10.2514/1.16399

[3] Eskridge, R. H., Fimognari, P. J., Martin, A. K., and Lee, M. H., "Design and Construction of the PT-1 Prototype Plasmoid Thruster," *AIP Conference Proceedings*, Vol. 813, No. , 2006, pp. 474–483. doi:10.1063/1.2169225

[4] Kirtley, D., Gallimore, A. D., Haas, J., and Reilly, M., "High Density Magnetized Toroid Formation and Translation Within XOCOT: An Annular Field Reversed Configuration Plasma Concept," 30th International Electric Propulsion Conference, Florence, Italy, Electric Rocket Propulsion Soc. Paper 2007-41, Fairview Park, OH, Sept. 2007.

[5] Slough, J., Kirtley, D., and Weber, T., "Preliminary Performance Measurements of the Air-Breathing ELF Thruster," *Joint Army, Navy, NASA, Air Force (JANNAF) Propulsion Meeting* [CD-ROM], Orlando, FL, Chemical Propulsion Information Analysis Center, Johns Hopkins Univ., Columbia, MD, 2008.

[6] Jahn, R. G., *Physics of Electric Propulsion*, McGraw–Hill, New York, 1968, p. 306.

[7] Dailey, C. L., and Lovberg, R. H., "The PIT MkV Pulsed Inductive Thruster," NASA CR 191155, July 1993.

[8] Lovberg, R. H., and Dailey, C. L., "A PIT Primer," RLD Associates, TR 005, Lebanon, PA, 1994.

[9] Dailey, C. L., and Lovberg, R. H., "Current Sheet Structure in an Inductive-Impulsive Plasma Accelerator," *AIAA Journal*, Vol. 10, No. 2, 1972, pp. 125–129. doi:10.2514/3.50076

[10] Lovberg, R. H., "Investigation of Current-Sheet Microstructure," *AIAA Journal*, Vol. 4, No. 7, 1966, pp. 1215–1222. doi:10.2514/3.3651

[11] Dailey, C. L., "Plasma Properties in an Inductive Pulsed Plasma Accelerator," 6th Biennial AIAA/Northwestern University Gas Dynamics Symposium, Evanston, IL, AIAA Paper 1965-0637, Aug. 1965.

[12] Dailey, C. L., "Investigation of Plasma Rotation in a Pulsed Inductive Accelerator," AIAA 6th Aerospace Sciences Meeting, New York, AIAA Paper 1968-0086, Jan. 1968.

[13] Dailey, C. L., "Investigation of Plasma Rotation in a Pulsed Inductive Accelerator," *AIAA Journal*, Vol. 7, No. 1, 1969, pp. 13–19. doi:10.2514/3.5028

[14] Spitzer, L., *Physics of Fully Ionized Gases*, Interscience, New York, 1956.

[15] Dailey, C. L., "Pulsed Electromagnetic Thruster," TRW Systems Group, AFRPL-TR-71-107, Redondo Beach, CA, Dec. 1971.

[16] Dailey, C. L., and Davis, H. A., "Pulsed Plasma Propulsion Technology," TRW Systems Group, AFRPL-TR-73-81, Redondo Beach, CA, July 1973.

[17] Dailey, C. L., and Lovberg, R. H., "Large Diameter Inductive Plasma Thrusters," 14th AIAA/DGLR International Electric Propulsion Conference, Princeton, NJ, AIAA Paper 1979-2093, 1979.

[18] Lovberg, R. H., and Dailey, C. L., "A Lightweight Efficient Argon Electric Thruster," 16th AIAA/JSASS/DGLR International Electric Propulsion Conference, New Orleans, LA, AIAA Paper 1982-1921, Nov. 1982.

[19] Dailey, C. L., and Lovberg, R. H., "Thrust Balance Performance Data for a One-Meter Pulsed Inductive Thruster," 17th JSASS/AIAA/DGLR International Electric Propulsion Conference, Tokyo, Electric Rocket Propulsion Soc. Paper 84-54, Fairview Park, OH, May 1984.

[20] Dailey, C. L., and Lovberg, R. H., "Pulsed Inductive Thruster Component Technology," TRW Space and Technology Group, AFAL-TR-87-012, Redondo Beach, CA, April 1987.

[21] Dailey, C. L., and Lovberg, R. H., "PIT Clamped Discharge Evolution," TRW Space and Technology Group, AFOSR-TR-89-0130, Redondo Beach, CA, Dec. 1988.

[22] Lovberg, R. H., and Dailey, C. L., "Current Sheet Development in a Pulsed Inductive Accelerator," 25th AIAA/SAE/ASME/ASEE Joint Propulsion Conference, Monterey, CA, AIAA Paper 1989-2266, June 1989.

[23] Lovberg, R. H., and Dailey, C. L., "PIT Mark V Design," AIAA/NASA/OAI Conference on Advanced SEI Technologies, Cleveland, OH, AIAA Paper 1991-3571, Sept. 1991.

[24] Mikellides, P. G., "Numerical Simulations of the Pulsed Inductive Thruster," 38th AIAA/SAE/ASME/ASEE Joint Propulsion Conference, Indianapolis, IN, AIAA Paper 2002-3807, July 2002.

[25] Polzin, K. A., and Reneau, J. P., "Effect of Conductive Walls on the Performance of a Pulsed Inductive Thruster," *IEEE Transactions on Plasma Science*, Vol. 37, No. 2, 2009, pp. 359–364. doi:10.1109/TPS.2008.2009987

[26] LaPointe, M. R., and Sankovic, J. M., "High Power Electromagnetic Propulsion Research at the NASA Glenn Research Center," *AIP Conference Proceedings*, Vol. 504, 2000, pp. 1538–1543. doi:10.1063/1.1290978

[27] Hrbud, I., LaPointe, M., Vondra, R., Dailey, C. L., and Lovberg, R., "Status of Pulsed Inductive Thruster Research," *AIP Conference Proceedings*, Vol. 608, 2002, pp. 627–632. doi:10.1063/1.1449781

[28] Frisbee, R. H., "Evaluation of High-Power Solar Electric Propulsion Using Advanced Ion, Hall, MPD, and PIT Thrusters for Lunar and Mars Cargo Missions," 42nd AIAA/SAE/ASME/ASEE Joint Propulsion Conference, Sacramento, CA, AIAA Paper 2006-4465, July 2006.

[29] Poylio, J. H., Russell, D., Goldstein, W., Jackson, B., Lovberg, R. H., and Dailey, C. L., "Pulsed Inductive Thruster: Flightscale Proof of Concept Demonstrator," 40th AIAA/SAE/ASME/ASEE Joint Propul-

sion Conference, Fort Lauderdale, FL, AIAA Paper 2004-3640, July 2004.
[30] Russell, D., Poylio, J. H., Goldstein, W., Jackson, B., Lovberg, R. H., and Dailey, C. L., "The PIT Mark VI Pulsed Inductive Thruster," Space 2004 Conference, San Diego, CA, AIAA Paper 2004-6054, Sept. 2004.
[31] Frisbee, R. H., and Mikellides, I. G., "The Nuclear Electric Pulsed Inductive Thruster (NuPIT): Mission Analysis for Prometheus," 41st AIAA/SAE/ASME/ASEE Joint Propulsion Conference, Tucson, AZ, AIAA Paper 2005-3892, July 2005.
[32] Cassady, R. J., Frisbee, R. H., Gilland, J. H., Houts, M. G., LaPointe, M. R., Maresse-Reading, C. M., Oleson, S. R., Polk, J. E., Russell, D., and Sengupta, A., "Recent Advances in Nuclear Electric Propulsion for Space Exploration," *Energy Conversion and Management*, Vol. 49, No. 3, 2008, pp. 412–435. doi:10.1016/j.enconman.2007.10.015
[33] Choueiri, E. Y., and Polzin, K. A., "Faraday Acceleration with Radio-Frequency Assisted Discharge," 40th AIAA/SAE/ASME/ASEE Joint Propulsion Conference, Ft. Lauderdale, FL, AIAA Paper 2004-3940, July 2004.
[34] Polzin, K. A., "Faraday Accelerator with Radio-Frequency Assisted Discharge (FARAD)," Ph.D. Thesis 3147-T, Department of Mechanical and Aerospace Engineering, Princeton Univ., Princeton, NJ, 2006.
[35] Lovberg, R. H., Hayworth, B. R., and Gooding, T., "The Use of a Coaxial Plasma Gun for Plasma Propulsion," Convair/General Dynamics, TR AE62-0678, San Diego, CA, May 1962.
[36] Polzin, K. A., and Choueiri, E. Y., "Performance Optimization Criteria for Pulsed Inductive Plasma Acceleration," *IEEE Transactions on Plasma Science*, Vol. 34, No. 3, 2006, pp. 945–953. doi:10.1109/TPS.2006.875732
[37] Polzin, K. A., "Scaling and Systems Considerations in Pulsed Inductive Plasma Thrusters," *IEEE Transactions on Plasma Science*, Vol. 36, No. 5, 2008, pp. 2189–2198. doi:10.1109/TPS.2008.2003537
[38] Hallock, A. K., Choueiri, E. Y., and Polzin, K. A., "Current Sheet Formation in a Conical Theta Pinch Faraday Accelerator with Radio-Frequency Assisted Discharge," 30th International Electric Propulsion Conference, Florence, Italy, Electric Rocket Propulsion Soc. Paper 2007-165, Fairview Park, OH, Sept. 2007.
[39] Hallock, A. K., and Choueiri, E. Y., "Effect of Neutral Density on the Thrust of a Conical Theta Pinch FARAD," 44th AIAA/SAE/ASME/ASEE Joint Propulsion Conference, Hartford, CT, AIAA Paper 2008-5201, July 2008.
[40] Polzin, K. A., Rose, M. F., Miller, R., Best, S., Owens, T., and Dankanich, J., "Design of a Low-Energy FARAD Thruster," 43rd AIAA/SAE/ASME/ASEE Joint Propulsion Conference, Cincinnati, OH, AIAA Paper 2007-5257, July 2007.
[41] Polzin, K. A., Rose, M. F., Miller, R., and Best, S., "Laboratory-Model Integrated-System FARAD Thruster," 44th AIAA/SAE/ASME/ASEE Joint Propulsion Conference, Hartford, CT, AIAA Paper 2008-4821, July 20–23 2008.
[42] Polzin, K. A., Rose, M. F., and Miller, R., "Operational Characteristics and Plasma Measurements in a Low-Energy FARAD Thruster," 44th AIAA/SAE/ASME/ASEE Joint Propulsion Conference, Hartford, CT, AIAA Paper 2008-5011, July 2008.
[43] Ramrus, A., and Rose, M. F., "High-Voltage Spiral Generators," 1st IEEE International Pulsed Power Conference, IEEE Paper IIIC-9, 1976.
[44] Rice, J. W., Gripshover, R. J., Rose, M. F., and Vãn Wagoner, R. C., "Spiral Line Oscillator," U.S. Patent, 4,217,468, 1980.
[45] Hallock, A. K., and Polzin, K. A., "Design of a Microwave Assisted Discharge Inductive Plasma Accelerator," 46th AIAA/SAE/ASME/ASEE Joint Propulsion Conference, Nashville, TN, AIAA Paper 2010-6527, July 2010.
[46] Dankanich, J. W., and Polzin, K. A., "Mission Assessment of the Faraday Accelerator with Radio-Frequency Assisted Discharge (FARAD)," 44th AIAA/SAE/ASME/ASEE Joint Propulsion Conference, Hartford, CT, AIAA Paper 2008-4517, July 2008.
[47] Owens, T. L., "A Pulse-Compression-Ring Circuit for High-Efficiency Electric Propulsion," *Review of Scientific Instruments*, Vol. 79, No. 3, 2008, Paper 034701. doi:10.1063/1.2836329
[48] Birx, D. L., Das, P. P., Fomenkov, I. V., Partlo, W. N., and Watson, T. A., "Pulse Power Generating Circuit With Energy Recovery," U. S. Patent 5,729,562, 1998.
[49] Bernardes, J., and Merryman, S., "Parameter Analysis of a Single Stage Induction Mass Driver," 5th IEEE International Pulsed Power Conference, IEEE Paper PI-27, 1985, pp. 552–555.
[50] Mikellides, P. G., "Numerical Simulations of the Pulsed Inductive Thruster," 38th AIAA/SAE/ASME/ASEE Joint Propulsion Conference, Indianapolis, IN, AIAA Paper 2002-3807, July 2002.
[51] Mikellides, P. G., "Numerical Simulations of the Pulsed Inductive Thruster," *AIP Conference Proceedings*, Vol. 654, , pp. 540–546. doi:10.1063/1.1541337
[52] Allison, D. L., and Mikellides, P. G., "A High-Temperature, Thermal Non-Equilibrium Equation of State for Ammonia," *International Journal of Thermophysics*, Vol. 27, No. 3, 2006, pp. 794–819. doi:10.1007/s10765-006-0065-y
[53] Mikellides, P. G., and Neilly, C., "Modeling and Performance Analysis of the Pulsed Inductive Thruster," *Journal of Propulsion and Power*, Vol. 23, No. 1, 2007, pp. 51–58. doi:10.2514/1.22396
[54] Mikellides, P. G., and Ratnayake, N., "Modeling of the Pulsed Inductive Thruster Operating on Ammonia propellant," *Journal of Propulsion and Power*, Vol. 23, No. 4, 2007, pp. 854–862. doi:10.2514/1.26609
[55] Mikellides, P. G., and Villarreal, J. K., "High Energy Pulsed Inductive Thruster Modeling Operating with Ammonia Propellant," *Journal of Applied Physics*, Vol. 102, No. 10, 2007, Paper 103301. doi:10.1063/1.2809436
[56] Alfvén, H., "Collision Between a Nonionized Gas and Magnetized Plasma," *Reviews of Modern Physics*, Vol. 32, No. 4, 1960, pp. 710–713. doi:10.1103/RevModPhys.32.710
[57] Martin, A., and Eskridge, R., "Electrical Coupling Efficiency of Inductive Plasma Accelerators," *Journal of Physics D: Applied Physics*, Vol. 38, No. 23, 2005, pp. 4168–4179. doi:10.1088/0022-3727/38/23/005
[58] Polzin, K. A., "Scaling and Systems Considerations in Pulsed Inductive Plasma Thrusters," 30th International Electric Propulsion Conference, Florence, Italy, Electric Rocket Propulsion Soc. Paper 2007-192, Fairview Park, OH, Sept. 2007.

L. King
Associate Editor